MXene-nanocellulose composite development by hydrothermal method for supercapacitor application

Master's Thesis in Materials Chemistry

Department of Chemistry

Author:

Chen Sun

Supervisors:

Dr. Lokesh Kesavan

Prof. Carita Kvarnström

15.05.2023

Turku

The originality of this thesis has been checked in accordance with the University of Turku quality assurance system using the Turnitin OriginalityCheck service.

Master's thesis

Subject: Materials Chemistry
Author: Chen Sun
Title: MXene-nanocellulose composite development by hydrothermal method for supercapacitor application
Supervisors: Dr. Lokesh Kesavan, Prof. Carita Kvarnström
Number of pages: 51 pages
Date: 15.05.2023

Abstract

MXenes, as representative of two-dimensional (2D) materials, stand out unique in many applications. Among MXene family, $Ti_{n+1}C_nT_x$ is the most mentioned and used one, which displayed large surface area and high electrical conductivity, even higher than well-known graphene. Owing to these merits, $Ti_{n+1}C_nT_x$ is an excellent candidate as electrode material for energy storage application, such as supercapacitor. However, $Ti_{n+1}C_nT_x$ easily undergoes re-stacking together with poor flexibility and low mechanical strength, which limit its performance and application. Herein, cellulose nanofibers (CNF) were introduced in order to address these issues, which are expected to prevent the re-stacking and increase the strength and flexibility of composite film. Composites were prepared with MXene and different types of CNF by hydrothermal method, supposedly bringing good dispersion. The as-prepared high-charge CNF/MXene composite exhibited relatively low areal capacitance of 12.6 mF/cm^2 at applied current density of 1 mA/cm^2 while it maintained capacitance retention of higher than 90% after 1000 cycles, displaying good cycling stability. Besides, composite films with different mass ratios of MXene and CNF (10M:90C, 50M:50C, 70M:30C) were fabricated to investigate the optimal amount of MXene used for self-standing film electrode. It turned out that all the films did not show desirable conductivity. Spectroscopic analyses and comparisons of films, prepared by hydrothermal treatment and sonication, implied that the oxidation of Ti atoms within MXene during hydrothermal process might be the reason for low conductivity, whereas sonication worked better for homogeneous dispersion of MXene and CNF, further leading to uniform conductivity of composite film.

Keywords: MXene, nanocellulose, electrochemistry, energy storage

Table of contents

Acknowledgement

Herein I sincerely thank Dr. Lokesh Kesavan and Prof. Carita Kvarnström for supervising me in my whole project. Also, Dr. Pia Damlin for spectroscopic characterization and Ashwini Jadhav for supplying MXene material and offering considerable help for my experimental operations and analyses. Further, I would like to thank Prof. Chunlin Xu, & Dr. Xiaoju Wang's research groups for supplying high & low charged cellulose nanofibre hydrogels for our composite development. In addition, I appreciate the help very much from Aymeric Lagadec, Yu Zou and SachinKochrekar who have made my project go smoothly. Besides, the technician Mauri Nauma offered a lot of support for customized operations.

Abbreviations

CNF	cellulose nanofibers
PVA	polyvinyl alcohol
TEMPO	2,2,6,6- tetramethylpiperidinyl-1-oxyl
PPy	polypyrrole
PANI	polyaniline
PEDOT	poly (3,4-ethylenedioxythiophene)
PDDA	poly (diallyldimethylammonium chloride)
EMI	electromagnetic interference
OER	oxygen evolution reaction
ORR	oxygen reduction reaction
HER	hydrogen evolution reaction
CNC	cellulose nanocrystals
BNC	bacterial nanocellulose
MFC	microfibrillated cellulose
t-CNC	tunicate cellulose nanocrystals
APS	ammonium persulfate
TOCNC	TEMPO-oxidized cellulose nanocrystals
TGA	thermogravimetric analysis
NHS	N-hydroxylsuccinimide
DMF	dimethylformamide
PEO	polyethylene oxide
CNT	carbon nanotubes
rGO	reduced graphene oxide
GONS	graphene oxide nanosheets
PSS	poly(styrene sulfonate)
HC CNF	highly-charged cellulose nanofibers
LC CNF	lowly-charged cellulose nanofibers
DI water	deionized water
GCE	glassy carbon electrode
NMP	n-methyl-2-pyrrolidone
grafoil	graphite foil
CV	cyclic voltammetry
EIS	electrochemical impedance spectroscopy
GCD	galvanostatic charging and discharging
XRD	X-ray powder diffraction
FT-IR	Fourier-transform infrared spectroscopy

1 Introduction

In today's world, environmental pollution and emission of greenhouse gases are troubling the global society. Therefore, renewable energy resources are of great importance for the purpose of alleviating the situation. The utilization of solar, tide and wind energy can be found as alternative practical applications. For example, electricity supply, to some extent, can be reliant on these renewable energy resources. Nonetheless, it is noteworthy that direct utilization of these energy resources is inefficient since they are intermittent. To address this problem, energy storage systems are introduced along with excellent stability and high efficiency, in which supercapacitor plays its role. Supercapacitor features fast charging-and-discharging, high powder density as well as long-term stability, due to which it has become a research spotlight [1]. 1D and 2D materials, such as carbon nanotubes, graphene, have been used for fabrication of electrode in supercapacitor development based on their properties, and in many occasions they are also incorporated in to other species to achieve good performance [1]. In recent years, MXene, as one of 2D materials, has attracted much attention due to its high electrical conductivity and large surface area. For supercapacitor, it is also a promising candidate as electrode. To bring more flexibility and mechanical strength to MXene, organic polymers are often added to form composites. For example, polyvinyl alcohol (PVA) was reported to enhance flexibility and enlarge interlayer spacing of MXene by intercalation, which further facilitated ion transport [3]. PVA was selected due to its abundant hydroxyl groups on the backbone, interacting well with MXene [3]. Herein, 2,2,6,6- tetramethylpiperidinyl-1-oxyl (TEMPO) oxidized cellulose nanofibers were used to endow MXene with more flexibility. CNF is not electrically conductive, but it makes possible the preparation of flexible composite electrode with better mechanical properties [4]. In our present study, we have developed MXene-Cellulose nanofibres composites prepared by hydrothermal method, which was likely to be explored and applied for the first time in supercapacitor applications. The method was

expected to mix components well and produce a homogeneous dispersion under inert atmosphere in aqueous medium.

1.1 MXene

MXenes, well-known in recent years, are a growing group of 2D early transition metal carbides or nitrides and they have drawn increasing attention owing to their surface hydrophilicity and high metallic conductivity [5]. MXenes can be represented by $M_{n+1}X_nT_x$, in which 'M' refers to an early transition metal, 'X' to carbon and/or nitrogen and 'T' to surface functional groups, such as -F, -OH, =O, as shown in Figure 1 [6]. At present, $Ti_3C_2T_x$ is the most commonly used MXene material for research, which was discovered by Gogotsi et al. in 2011 for the first time [7]. The research group applied acid etching to obtain $Ti_3C_2T_x$ with the help of etchant HF.

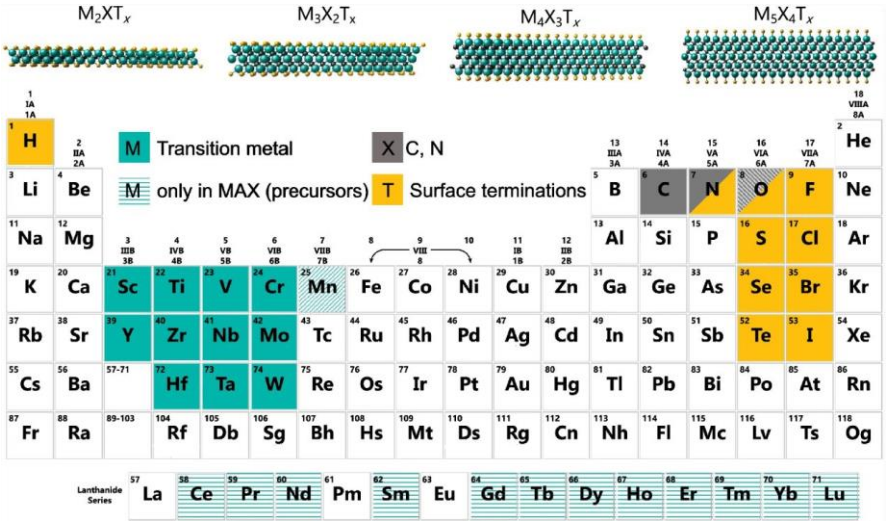

Figure 1. MXene comprised of elements displayed in the periodic table. Green block refers to transition metal (M); Gray block refers to carbon or nitrogen; Yellow block refers to surface elements; Green-line block refers to rare-earth element of MAX precursor [6].

It is noteworthy that MAX phase is generally perceived as precursor for MXene, in which here 'M' and 'X' stand for the same elements with those in MXene while 'A' refers mainly to elements belong to groups 13 and 14. In MAX phase, 'M' layer shows good interaction with 'X' layer by the formation of ionic, covalent and metallic bonds while it shows weak interaction with 'A' layer resulting from the formation of only

metallic bonds. Thus, 'A' layer can be removed with more ease. By addition of HF, 'A' layer between two MX layers can be etched away in the form of fluoride. For $Ti_3C_2T_x$, the precursor Ti_3AlC_2 converts into $Ti_3C_2T_x$ after being treated with HF, of which the process is illustrated in Figure 2 [7]. However, the utilization of HF is limited due to its toxicity and being harmful to the human body and environment, whereupon a proper combination of acid and fluoride is applied for etching, replacing HF [5].

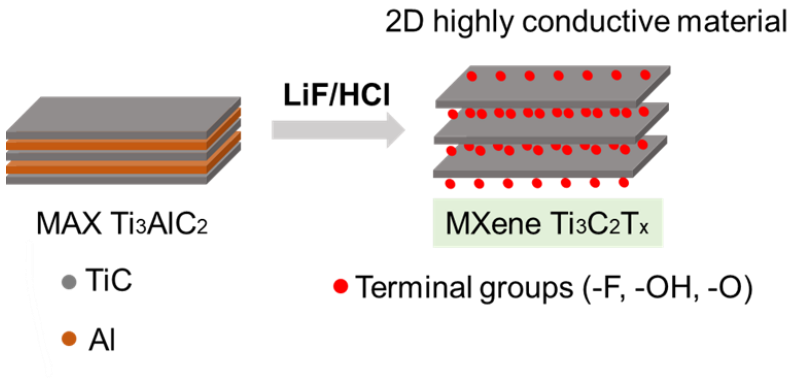

Figure 2. Schematics of etching process of MAX by HF [7].

For example, LiF/HCl has been used by many research groups, and well-etched MXenes were obtained [3]. In this case, concerns with co-existence of highly concentrated hydrogen ion and fluorine ion still stand, which likely leads to release of HF. To produce MXene in a more environment-friendly way, bifluorides, a sort of weak acids, are subsequently selected, which mainly consist of NH_4HF_2, KHF_2 and $NaHF_2$ [5]. The cations of these bifluorides are capable of enlarging the spacing between MXene layers via intercalation, which further changes the physical properties of MXene [8]. Though $Ti_{n+1}C_nT_x$ is representative of MXene family, MXene containing nitrogen is explored as well. To synthesize N-containing MXene, fluorine-containing acid is insufficient for removal of N phase since Ti-N bonds exhibit more strength and $Ti_{n+1}NnT_x$ shows a tendency to dissolve in acid etchant [9]. Instead, molten salts, such as LiF, KF and NaF, work well in this case [5]. Moreover, fluorine groups can be unfavorable in certain occasions owing to its chemical inertness, so fluorine-free synthesis method is developed when fluorine groups are not expected on MXene. For example, alkaline solution with high concentration was used to treat MAX precursor in

hydrothermal way, leaving no fluorine groups after removal of 'A' phase in the form of aluminate and hydroxide, as displayed in Figure 3 [10]. In addition, a novel bottom-up synthesis approach was proposed, which was to use chemical vapor deposition to form MoC_2 with methane as carbon source and Cu-Mo alloy as metal source. When temperature was increased, two separate metals melted, followed by formation of alloy at the interface, and the melted Mo moved towards the surface of alloy to react with methane [11].

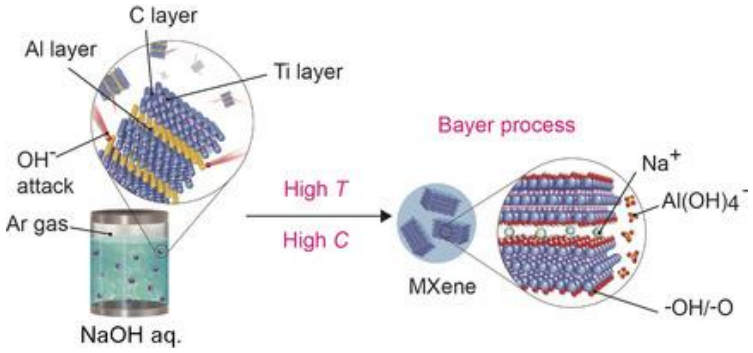

Figure 3. Schematics of treating MAX phase with NaOH by hydrothermal method[10].

MXenes have diverse unique properties as a result of electronic structures, atomic and layer stacking, surface functional groups, etc. [12]. High electrical conductivity, and hydrophilicity are characteristics of MXenes, which are also features of interest that this research project is looking at. To be used as electrode in a supercapacitor, there is a prerequisite that the material shows good conductivity. Conductivity with a range from 850 to 15000 S cm^{-1} has been reported for $Ti_{n+1}C_nT_x$ [13], which can be tuned by surface functionalization, change in chemical composition as well as structural transformation. For instance, the conductivity decreases with the increasing number of MXene layers and terminal groups [12]. In addition, it is noteworthy that etching methods, as mentioned above, also have effect on electric properties of MXene. Treatment in alkaline solution at high temperature can remove inert fluorine groups on the surface of MXene, subsequently leading to higher conductivity. Also, shorter etching time together with lower etchant concentration produces MXene with lower defect density and increased flake sizes, which enhance conductivity as a result [14]. Moreover, other properties, such as thermal, mechanical and optical properties, are

influenced by various factors, and by adjusting these factors MXenes can be adjusted into a wide range of applications.

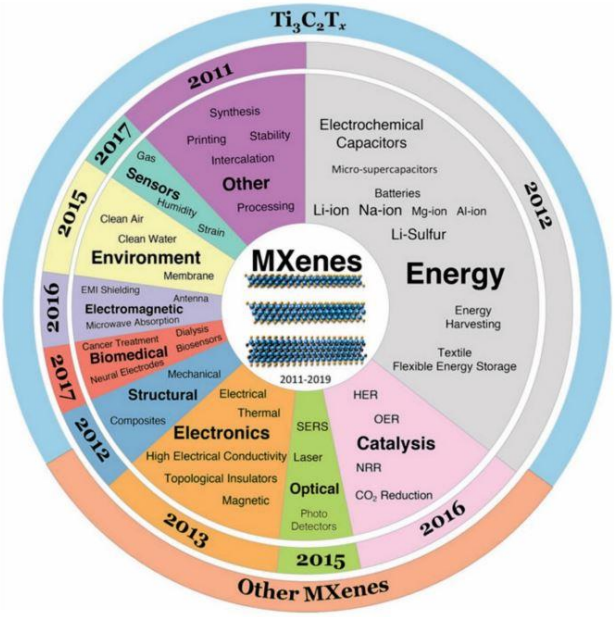

Figure 4. The applications of MXenes based on their properties [15].

1.2 Applications of MXenes

When it comes to applications of MXenes, various fields can benefit from them owing to their unique properties (biological, physical and chemical properties) (Figure 4) [15]. Among these applications, the significance of MXenes has been demonstrated in energy storage devices, such as supercapacitor and battery. In case of supercapacitors, MXenes were previously reported to bring high specific capacitance, acting as electrodes in the system [16]. Theoretical studies on MXenes showed the relevance of their electrical conductivity with elemental composition and surface functional groups on MXene nanosheets. By modifying terminal groups electrical properties of MXenes can be tuned [17]. In order to facilitate the ion transport in the $Ti_{n+1}C_nT_x$-based electrode, Chen's group proposed a terminal-removal method, in which $Ti_{n+1}C_nT_x$ was treated with alkaline solution and high temperature annealing in sequence to remove unfavorable -F and -OH groups that hinder mass transport [18]. Nonetheless, -F and -OH groups also benefit MXene films in terms of mechanical properties, which protect the layered

structure and improved mechanical elasticity, featuring enhanced tolerance towards tensions [19]. Ghidiu' group developed MXene electrode by rolling the prepared clay-like MXene into flexibility film. Via electrochemical analyses, pseudocapacitive (Faradaic) current was observed for MXenes, in addition to capacitive current. It was thought to result from insertion of protons in the acidic electrolyte, which further leads to the changes in the reversible oxidation states of Ti atoms at the surface and allows the storage of extra charges for enhanced capacitance [20]. Other factors of affecting capacitance were investigated as well. Surfactant that interacts well with terminal groups was utilized on $Ti_{n+1}C_nT_x$ surface to help form and maintain a vertical alignment of MXene nanosheets, which endowed the electrode with shorten pathways for mass transport than parallel alignment of MXene, as depicted in Figure 5 [21].

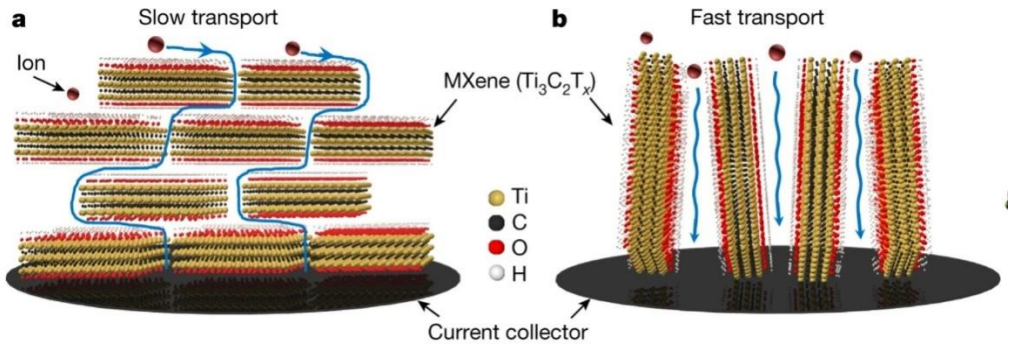

Figure 5. Schematic of (a) parallel alignment of MXene nanosheets and (b) vertical alignment of MXene nanosheets[21].

Moreover, growing efforts have also been made to seek for suitable alternative materials as electrode in battery, among which MXenes stand out. For example, the well-known "shuttle effect", existing in lithium-sulfur battery, tends to cause poor cycling stability and the loss of active species in electrode, which can be suppressed with the help of $Ti_{n+1}C_nT_x$[22]. During cycles of charging and discharging, lithium polysulfide is formed at the sulfur electrode, and subsequently dissolves into electrolyte and moves between two electrodes, which become an inactive phase eventually. By using $Ti_{n+1}C_nT_x$to prepare MXene/S electrode, the formed polysulfide could be immobilized in MXene through chemisorption and interact with surface functional groups to produce a protective thiosulfate complex layer, which enhanced the cycling

stability and the utilization of electrode material [22]. Besides, MXenes was also theoretically proved to allow swift sodium-ion diffusion, indicating their application prospects in sodium-ion batteries [23]. Moreover, MXene suffers from re-stacking behavior of MXene nanosheets due to interlayer interaction, which can block mass transport within the electrode and limit its performance in application. Therefore, additives are introduced to prevent re-stacking and enlarge the interlayer spacing. In most cases, polymers are typical additives. For instance, in order to enhance the accessibility to active sites, polyvinyl alcohol (PVA) was selected for hybridization with MXene owing to its high solubility in water and adequate hydroxyl groups along the polymer chain [24]. The prepared composite film exhibited improved tensile strength and flexibility compared to MXene film, and showed increased volumetric capacitance of ca.530 F/cm^3, which was believed to derive from larger interlayer spacing between MXene nanoflakes by intercalation of PVA and cations in the electrolyte [24]. Wang's research group mixed bacterial cellulose with MXene, which resulted in a composite film with excellent tensile strength and high specific capacitance, which might be ascribed to interconnected nanofiber network, further facilitating the charge transfer through these existing pathways. Also, conductive polymers are considered for composite fabrication due their electrical conductivity. Pyrrole was previously polymerized into MXene interlayers, after which conductive polypyrrole (PPy) was formed between, as depicted in Figure 6 [26]. The PPy was expected to serve as interlayer spacer, and increased the number of channels for charge transfer. Similarly, polyaniline (PANI) showed remarkable potential in improving the ability of charge storage for MXene film. Armin's research group fabricated PANI/$Ti_3C_2T_x$ self-standing composite films by polymerization of aniline monomers onto MXene sheets with controlled thickness [27]. Not only did the prepared film exhibit high specific capacitance but also it showed outstanding cycling stability [27]. The performance of battery electrode can be improved with the introduction of polymer additives as well. PEDOT (poly (3,4-ethylenedioxythiophene))/MXene electrode for lithium-ion battery was reported to have more kinetically favorable interface redox

reactions, electrolyte ion diffusion and more pronounced interlayer separation of MXene, which contributed to the enhancement in both reversible capacity (ca.300 mA·h/g) and long-term stability after hundreds of cycles when compared to MXene and PEDOT electrodes [28]. Besides, in order to combine and fully utilize the advantage of high-capacity black phosphorene, the hybridization of MXene and black phosphrene together with poly(diallyldimethylammonium chloride)(PDDA) was proposed for sodium-ion battery electrode, and was proved to endow the battery with excellent capacity as well as cycling stability [29].

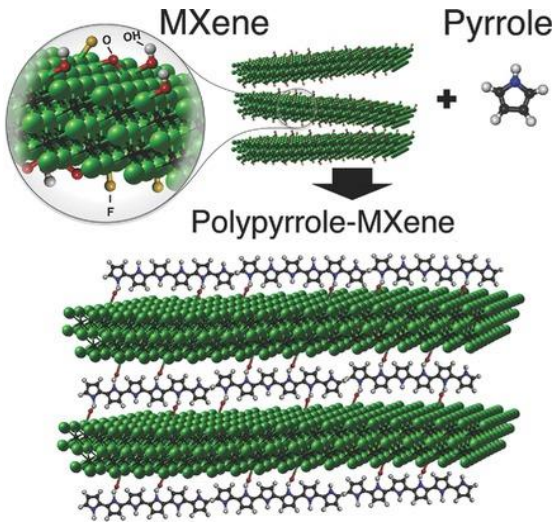

Figure 6. Demonstration of pyrrole polymerization between MXene layers [26].

In addition to applications for energy technology, MXenes' use for other purposes is also drawing growing attention. As is widely known, efficient gas separation plays a pivotal part in industrial manufacturing and household use that involve filtering impurities and unwanted gas components from original natural gas or biogas. In today's world being threatened by global warming, removal of CO_2 becomes increasingly important for the purpose of achieving sustainability, to which MXenes materials can make contribution to. For gas separation, surface functional groups and interlayer spacing of MXene determine its capability of sieving gas molecules. Pristine MXenes were reported to be highly H_2-selective with low CO_2 penetration, which could be ascribed to "trapping effect" of CO_2 within MXene by interaction (attached and de-attached) with oxygen-containing terminal groups between layers [30]. Interestingly,

functionalizing the surface with borate and amine could cause interlayer separation to narrow down, and the trapping effect of oxygen-containing groups was eliminated, which led to notable CO_2 selectivity of MXene, as illustrated in Figure 7 [30]. When gas separation is discussed, liquid separation using MXenes cannot be ignored. Liquid separation shares the similar mechanism, which is to modify the sieving properties based on the target liquid molecules. For instance, with consideration that MXene surface is negatively charged, cations were intercalated into MXene layers, and formed stable broadened transport channels for molecules with a specific range of diameters [31].

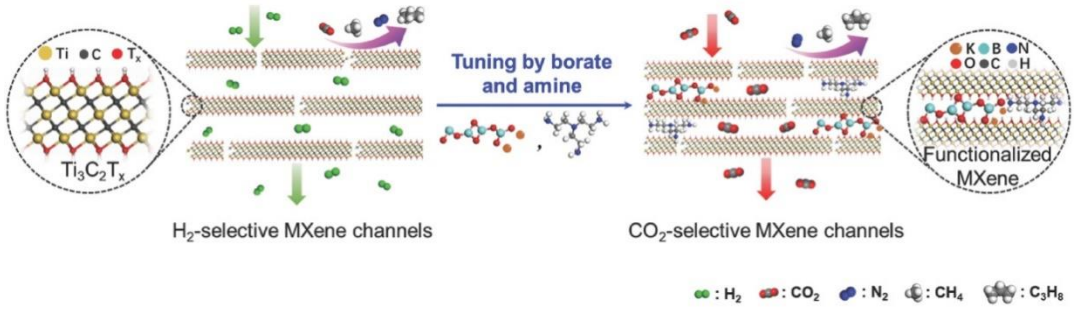

Figure 7. Schematic of change in gas sieving properties before and after surface modification of MXene [30].

Another potential application that MXenes stand out for is electromagnetic interference (EMI) shielding. Materials that display EMI effect have tremendously promising prospects in applications in our daily life. For example, in summer time, windows coated with such materials can block the heat energy transmitting through to the room space, so it takes less energy to cool down the temperature inside the room with air conditioner. A prerequisite for great shielding behavior is that material should have continuous electrical conductivity, in which charge carriers facilitate the reflection of radiations [32]. Based on this principle, MXenes are a suitable candidate owing to their electrical properties. It was reported that shielding properties of MXenes derived from reflection and absorption of electromagnetic waves by their charge carriers (transition metals and/or carbon) and surface functional groups [33]. When radiation penetrates into MXene layers, it will be reflected internally and vanish with gradual attenuation of intensity, as demonstrated in Figure 8 [33].

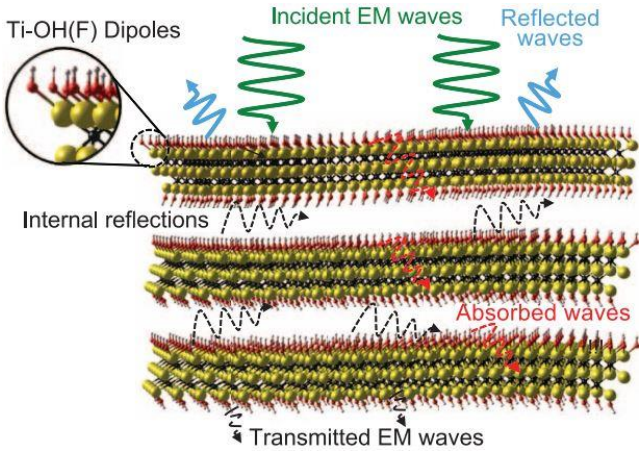

Figure 8. Schematic of mechanism of EMI shielding of MXene [33].

Besides the applications mentioned above, MXene-based electrocatalysts also exhibit superior activity for oxygen evolution and reduction reaction (OER/ORR) and hydrogen evolution reaction (HER). Kiran's group prepared vanadium carbide V_2C with HF etchant, which led to remarkable bifunctional ORR/OER electrocatalytic activity with low overpotentials, compared with its MAX phase precursor [34]. Exclusively, =O terminated titanium carbide was reported to be an excellent electrocatalyst for HER with more positive onset potential (with reference to an overpotential of -0.19 V at the current density of 10 mA/cm^2) and lower Tafel slope compared to multiple-termination in MXene [35]. Also, it is noteworthy that MXenes possess antibacterial properties owing to their capability of inhibiting nutrient uptake of bacteria via bonding with their surface, and in recent years the use of MXenes in this field has drawn more and more attention among biochemists [36]. Anyway, MXenes can find their place based on their various properties. In this project, the electrical conductivity of MXene hybrids is utilized and investigated with regards to energy storage.

1.3 Nanocellulose

As one of the most abundant polymers (polysaccharide), cellulose can be found in a broad range of plants and living organisms at microscale. From the perspective of

chemical composition, linear and continuous β-D-glucose units make up cellulose via the formation of β-(1,4) glycoside, of which the configuration is shown in Figure 9. The number of repeated units ($(C_6H_{10}O_5)_n$) empirically vary from 10000 to 15000 replying on the categories of cellulose precursors [39]. In cellulose, anhydroglucose six-member rings are linked via the formation of covalent oxygen bonding between two carbon atoms at two neighboring units, as well illustrated in Figure 9. It is widely acknowledged that terminal-rich polymers chains can interact internally, which contributes to the change in the entire configuration. Cellulose undergoes similar configuration changes. Hydroxyl groups can interact with each other (and oxygen atoms) to form intrachain and interchain hydrogen bonding, which helps to stabilize mesh-like structure as well as cellulose chains. It is not difficult to realize that this kind of interaction explains parallel arrangement of couples of cellulose chains, which are able to gather line-by-line into fibrils. The network structure of cellulose makes it a stable polymeric matrix with high axial stiffness [39]. In trees, plants, microbes and marine living creatures, cellulose is one of the key components to maintain their interior or exterior structures since cellulose fibrils exhibit strength and effective reinforcement to the whole structure. Interestingly, cellulose has domains of different crystallinity, much like carbon materials. Crystalline structure is observed where cellulose chains are arranged with high degree of order while amorphous structure exists where chains are disordered.

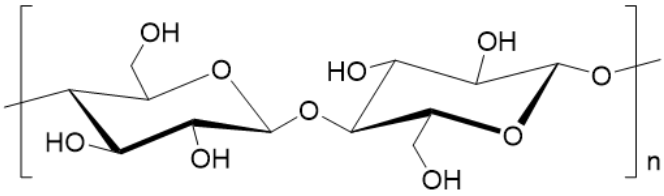

Figure 9. Cellulose consisting of glucose monomers.

The regions containing crystalline cellulose are classified into four types, tagged with Greek numbers (I, II, III and IV), and type III and IV can be further subdivided into III_1, III_{11} and IV_1, IV_{11}, respectively [40]. Cellulose I is perceived as natural cellulose because it derives from natural production of a wide spectrum of living organisms, this

type of cellulose has metastable structure in thermodynamic view as it can be transformed into other sorts of crystalline cellulose such as cellulose II and III [39]. Cellulose II with monoclinic structure has so far the most stable structure and has been widely studied, which can be produced from cellulose I by two methods: 1) regeneration, in which cellulose II is generated after solubilization and precipitation of cellulose I in a solvent; and 2) mercerization, in which cellulose II is formed by swelling cellulose fibers in aqueous sodium hydroxide [39]. Cellulose III_I as well as III_{II}originates from cellulose I and II via treatment in liquid ammonia and some kinds of amines, followed by evaporation of excessive reagents.[40] Through further treatment of cellulose III_I and III_{II}, in-glycerol at high temperature (over 200 °C) cellulose IV_I and IV_{II} are yielded [40]. The polymorphs of crystalline celluloses can be interconverted through effective treatments, as detailed in Figure 10 [40].

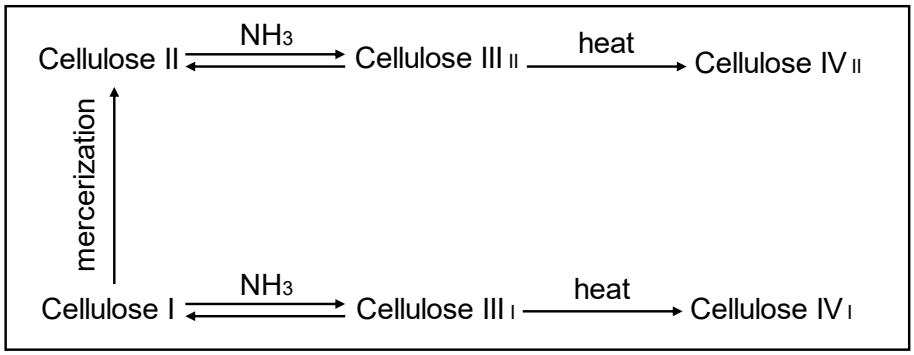

Figure 10. Illustration of transformation of different polymorphs of cellulose [40].

Among these crystal structures of celluloses, cellulose I is of high significance in this master project as the signals corresponding to the cellulose I are observed for data comparisons. When looking more into cellulose I, triclinic structure (Iα) and monoclinic structure (Iβ) stand for polymorphs of type I [39]. These two polymorphs with different proportions are the dominating structures that can be found in various sources of cellulose. It is noteworthy that Iα phase is relatively less stable compared to Iβ, which enables it to change towards the Iβ phase under certain conditions, like thermal process in aqueous alkaline solution or in organic solvents with inert gas atmosphere [39]. Besides, manipulation on the proportion of Iα and Iβ can be achieved through changing the process conditions, such as temperature, the concentration of

solution and so on [39]. Based on the typical crystal structure of cellulose I, characterization techniques help to detect its existence. The crystallinity of cellulose was firstly proposed by Carl in 1858 when polarizing microscope was employed[40]. Later in 1930s powder X-ray crystallography proved it to be valid, and more extensive investigation on the crystal structure of cellulose began, during which several models of unit cells with proposed parameters were discussed [40]. The obtained crystallinity of cellulose I is affected by dozens of factors: technical conditions, cellulose source, degree of crystallinity and sample purity [40]. In this project, characteristic peaks referring to cellulose I structure were observed and analyzed.

Now that cellulose has crystalline regions, but amorphous domains also should be mentioned. There is a record that wide-angle X-ray scattering was applied to visualize any structure belonging to amorphous phase of cellulose. In diffraction patterns of cellulose, crystalline phase is reflected by light area, and to the stark contrast amorphous cellulose displays an obvious dark area [40]. However, this observation might not be properly interpreted as a curvature along the cellulose fibrils can influence the diffraction of certain regions, which invalidate the color-based standards used for differentiating crystalline and amorphous phases in cellulose matrix [40]. It was pointed out that surface fibrils construct the amorphous phase of cellulose, or in other words, proportion of surface hydroxyl groups indicates the content of amorphous cellulose [40]. For example, a crystallinity of microbial cellulose is analyzed to be over 70% with a crystal dimension of around 5 nm, in which case crystal surface harbors approximately 36 chains and therefore brings a certain degree of amorphous cellulose [40]. Practically, amorphous cellulose does not refer to the fully amorphous phase while cellulose still shows crystallinity at some level at the same region instead [40].

As mentioned above, cellulose can be obtained from various sources. The most common and abundant source material is wood. Extraction of cellulose from wood can be readily accessible since harvesting and following processing (into products) can be

efficiently achieved with the aid of a set of industrial machines, and in most cases, wood is purified to pulp by eliminating the majority of lignin, impurities as well hemicellulose before processing [39]. Other plants, such as cotton, wheat straw, soybean stock, make extraction of cellulose possible for the same reason for wood. Therefore, it can be inferred that plants are a popular option for getting cellulose. However, what's eye-catching is that some animals are also able to generate cellulose microfibrils. As a group of sea animals, tunicates are equipped with a piece of thick "clothes" comprising cellulose and protein, and this outer phase exactly provides cellulose microfibrils [39]. Tunicates can be divided into different classes, on which the production process and microstructure of cellulose fibrils rely heavily [39]. Besides, within the region of cell walls cellulose is produced by different categories of algae, in which biosynthesis plays a pivotal part [39]. Last but not the least, bacteria are competent candidates for cellulose production, in which Gluconacetobacterxylinus gains the most attention from researchers. Though the underlying reason for generation of cellulose remains unknown, cellulose is believed to protect bacteria from damage caused by irradiation (e.g., ultraviolet light) and other microbes [39]. As bacteria produce cellulose under suitable culturing conditions, this advantage can be well taken to change structure and crystallinity of the resulting cellulose by changing culturing conditions accordingly [39].

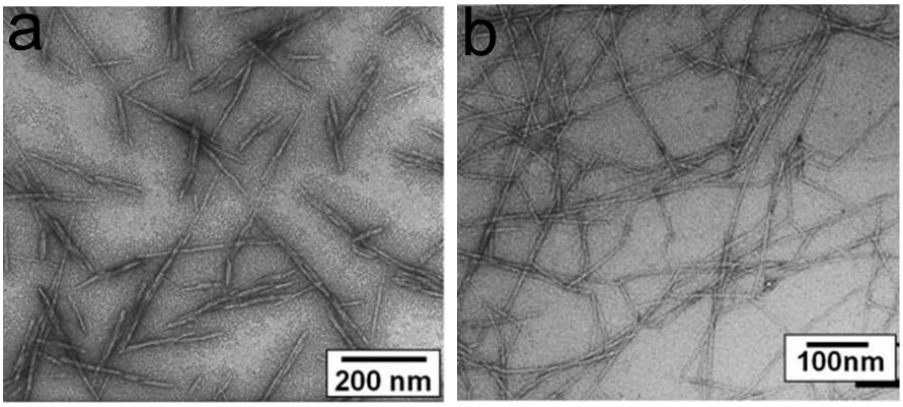

Figure 11. TEM images of (a) cellulose nanocrystals from wood; (b) TEMPO-treated cellulose nanofibers [39].

When it comes to nanocellulose, it refers literally to cellulose (at least one dimension) in the nanoscale, and it can be present in diverse morphologies, sizes, and crystallinity

[39]. Nanocellulose primarily includes often-heard rod-like cellulose nanocrystals (CNC) shown in Figure 11a, chain-like cellulose nanofibers (CNF) shown in Figure 11b, bacterial nanocellulose (BNC) and less-mentioned kinds of nanocellulose, such as microfibrillated cellulose (MFC), tunicate cellulose nanocrystals (t-CNC) [39].

Among all the nanocelluloses stated above, cellulose nanocrystals are employed most frequently, and the main method to obtain CNC is to hydrolyze the amorphous domains existing in cellulose fibers [41], in which aqueous alkaline solution (NaOH) or bleaching is applied to remove various impurities in raw material like esters, hemicellulose and lignin, and then hydrolysis takes place in the acidic condition at high temperature to process the pretreated amorphous material into cellulose nanocrystals. After a period of hydrolysis, suspension of cellulose nanocrystals is collected, followed by centrifugation and dialysis for obtaining CNC.[41] The categories of source materials, hydrolysis reagents and conditions determine to a large extent, the dimensions of CNC with respect to length and diameter. For instance, after cotton fibers were hydrolyzed under temperature of 65 °C in sulfuric acid, the obtained CNC exhibited length and diameter with a range of 200 ~ 300 nm and 10 ~ 30 nm, respectively [41]. However, when ascidian was used as source material, the hydrolysis with the same temperature and reagent yielded CNC, whose length went beyond 1 μm [42]. It should be mentioned that if the hydrolysis undergoes incompletely, the prepared CNC might not be desirable products due to a reduction in crystallinity and a morphological deviation of CNC [39]. In addition to hydrolysis in acids, some chemicals, such as ammonium persulfate (APS), tetreamethyl-piperidin-1-oxyl (TEMPO), can react with cellulose to facilitate the production of CNC [41]. It is notable that TEMPO-mediated oxidation of cellulose works well from the perspectives of selectivity, reaction rate and cost of energy, in which hydroxyl groups are oxidized, and subsequently carboxyl groups are introduced onto cellulose fibrils (Figure 12). The process which promotes the release of nanofibrils is catalyzed by TEMPO species along with NaClO and NaBr [43]. Thereafter, the TEMPO-oxidized CNC (TOCNC) go

through centrifugation and dialysis for separation and purification of TOCNC from the obtained mixture [41].

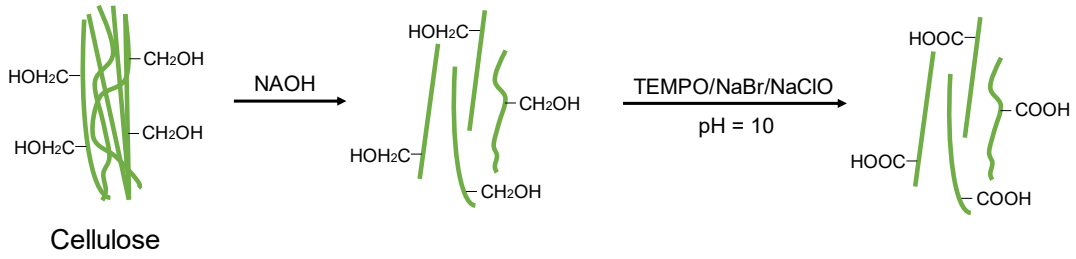

Figure 12. Schematic of TEMPO-oxidation of cellulose [43].

Cellulose nanofibers (CNF) with different morphology are another type of nanocellulose, which therefore requires different approaches from those for CNC. Literally, it is easier to prepare CNF than CNC since the CNC derives from the breakage of cellulose chain whereas there is no such change in molecular structure for CNF.[44] In practice, physical treatments can be applied to generate CNF from raw materials, which include ultrasonication, high-pressure homogenization as well as mechanical shearing and grinding [44]. With the help of added chemicals, alternative methods for such preparation are available. As mentioned above, the use of TEMPO oxidation benefits the preparation of cellulose nanocrystals, which works for CNF as well. For example, Tsuguyuki's group treated bleached kraft pulp from hardwood with different content of water, with TEMPO-aided oxidation, and subsequently stirred the obtained slurry to produce highly crystalline CNF with dimensions of width of ca. 4 nm and length of several microns [45]. They also found that a pH value of 10 might be efficient for oxidation, and the oxidation towards highly dense carboxyl groups on the CNF was crucial to maintain stability of the dispersion due to the existing electrostatic repulsion [45]. Moreover, the successful production of CNF can also be achieved by a combination of physical and chemical methods. Lar's group homogenized the carboxymethylated softwood cellulose at high pressure, which resulted in CNF [46]. The common source materials for CNF are wood as can be seen in quite a few experiments. Other materials, such as cotton fibers, are being under investigation for their feasibility of providing CNF. The different source materials own distinct

microstructures, further leading to the different scales of extracted cellulose nanofibers, as depicted in Figure 13 [47].

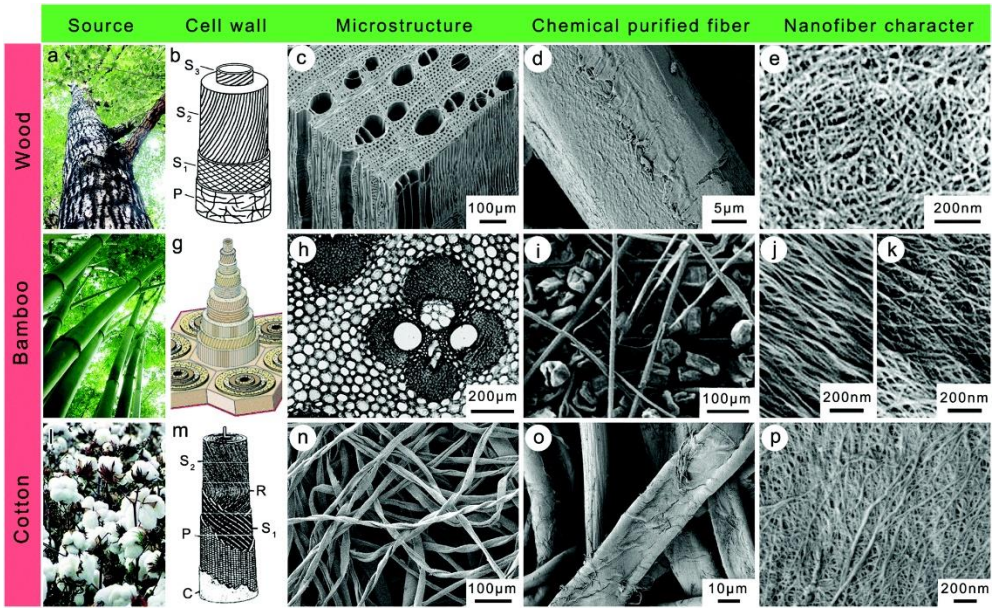

Figure 13. The morphologies of cellulose nanofibers in different source materials [47].

Bacterial nanocellulose (BNC), also a type of often-heard nanocellulose, draws a lot of attention due to its high purity. It is produced in natural way of fermentation process by some bacterial genera, such as Escherichia, Azotobacter, Sarcina, Acetobacter, Aerobacteras well as Rhizobium [44][47]. Interestingly, BNC itself can be used as source materials for a dessert nana-de-coco, in which BNC gel sheets obtained in coconut water are shaped accordingly and immersed in sugar syrup [47]. Compared to CNC and CNF, biosynthetic process dominates in the preparation of BNC. In the bacterial cell, β-1,4-glucan fibrils are firstly generated with the help of cellulose synthase, and then these fibrils pass through the cell membrane by bacterial extracellular excretion. Finally, excreted fibrils crystallize, aggregate and interconnect to further form a hydrogel of cellulose nanofibers with porous entangled web-like structure, the process of which is shown in Figure 14 [48]. Also, the structural features of BNC are determined, to a large extent, by the types of microbes, the nutrient contents in the culture medium and the production approaches [44][47]. With regards to the dimensions of BNC, it has width of ca. 100 nm and length of ca. 100 μm, shaped like ribbon [47]. It is noteworthy that functional groups, such as carbonyl and carboxyl, are

not present in BNC, and a high degree of cellulose purity can be expected in BNC [48]. Different preparation methods can endow BNC with various structures functioning in different ways, which include fermentation, genetic modification, strain engineering [44].

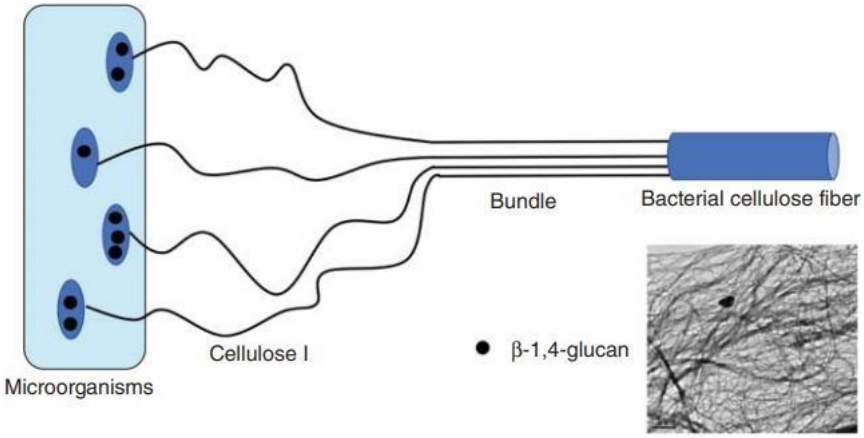

Figure 14. Schematic illustration of synthesis of bacterial nanocellulose [48].

Nanocellulose has been appealing to researchers owing to its diverse properties. One of the most significant properties is its excellent mechanical properties, which is represented by previously reported high Young's modulus and tensile strength of around 140 GPa and 3 GPa, respectively [49]. Typically, cellulose nanofibers with network structure are thought to display a high aspect ratio, which exactly serves as an origin of mechanical enhancer in CNF [44][47]. The source materials and the preparation strategies are factors affecting the mechanical properties of nanocellulose. For instance, extracted cellulose nanocrystals from tunicate exhibit a high Young's modulus while differently extracted cellulose nanofibers from the same source shows a drastic decrease in Young's modulus [44]. In this research project, cellulose nanofibers are used in order to improve the mechanical properties of MXene. Therefore, the mechanical properties of nanocellulose are well utilized and attached much importance. Also, thermal properties of nanocellulose draw considerable attention, when thermal stability is taken into consideration. Based on thermogravimetric analysis (TGA), it is within the temperature range of 200 ~ 300 ℃ that nanocellulose starts to degrade chemically and it is determined by the categories of nanocellulose, rate of temperature

elevation as well as modification on cellulose surface [39]. In terms of long-term use, thermal stability of nanocellulose-based materials is prioritized, to which nanocellulose can contribute, to a certain degree. In addition to mechanical and thermal characteristics, hydrophilicity poses as another feature of nanocellulose. As a huge number of hydroxyl groups exist along the backbone chain of cellulose nanofibers, CNF is endowed with pronounced hydrophilicity, which provides means of further chemical or physical modification such as replacement and halogenation of hydroxyl groups, or physical mixture with other components via the formation of hydrogen bonding. Furthermore, large specific surface area can be expected in nanocellulose, which is brought by its mesh-like structure [39].

Prior to the use of nanocellulose, surface modification, in some occasions, is preferred or even required. Several approaches, such as esterification, oxidation (Figure 15) and physical modification, are available to modify the properties of nanocellulose with high degree of control. Uniform dispersion of nanocellulose is a prerequisite for high-quality surface modification, which can be achieved by use of organic solvent and physical treatment like ultrasonication-assisted homogenization [47].

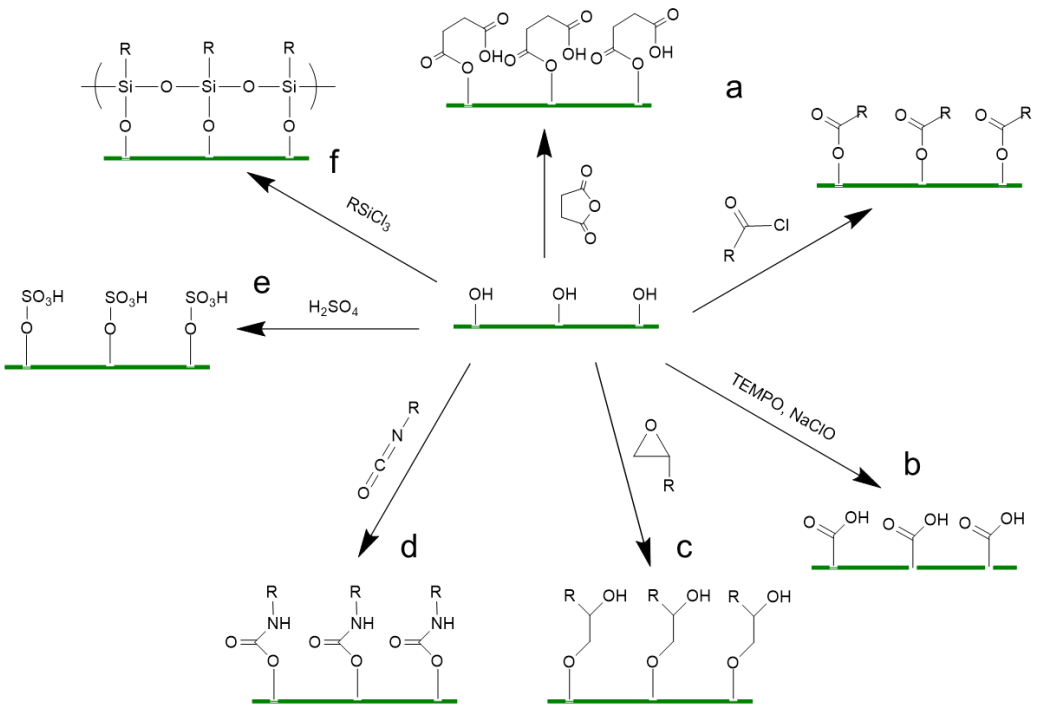

Figure 15. Chemical modification of nanocellulose. (a) Esterification with acid anhydride and carboxylic acid chloride; (b) TEMPO-mediated oxidation; (c) Etherification with epoxide; (d) Amidation; (e) Sulfonation; f. silylation.

Esterification is the most frequently used among these methods, in which a large proportion of hydroxyl groups are converted to esters with crystalline structure of nanocellulose intact [50]. When hydrophobic nanocellulose is favorable in research, esterification can be applied, by which the mechanical properties are improved with comparison to hydrophobic polymers containing no this kind of treated nanocellulose [44]. Similarly, etherification replaces hydroxyl groups with ethers though there is a pronounced difference from esterification that etherification is less efficient due to the polymerization of reagents [44]. Reaction conditions can be altered to mitigate the polymerization, while it is still hard to entirely eliminate [44]. When carboxylated nanocellulose is desired, oxidation is definitely an effective choice. As mentioned previously, TEMPO plays a key role in oxidation of nanocellulose, in which hydroxyls groups are selectively oxidized to carboxyl groups. Meanwhile, it should be noted chemical linkage between cellulose units may be destroyed when applied with highly concentrated TEMPO and long-time reaction, which results in the formation of smaller pieces of nanocellulose and loss of degree of crystallinity. Compared to TEMPO, APS

is less favorable because the crystalline structure of nanocellulose is likely to be disturbed or destroyed tremendously by APS oxidation [44]. Besides carboxylation, nanocellulose also allows its hydroxyl groups to be substituted with aldehyde groups, for which the oxidant sodium periodate ($NaIO_4$) is employed. After this replacement, the formed aldehyde groups are still reactive towards further chemical species, culminating in a high control on surface properties of nanocellulose that is otherwise difficult to attain with functional hydroxyl groups. Amidation, in which amine and carboxyl groups are linked, is also a feasible way to modify the surface of nanocellulose. With considerations that amine species exist widely in a spectrum of biomolecules, they stand out as amine providers [44]. In many cases, carboxylation or amination of nanocellulose is supposedly finished ahead of amidation since nanocellulose contains neither of those two functional groups before any possible modification. With respect to the process, it depends on the additives used. When nanocellulose is modified step-by-step in aqueous solutions, N-hydroxylsuccinimide (NHS), as an "activator", can facilitate the carboxylated nanocellulose to interact with amine providers to fulfill amidation; while in one-step synthesis the additive like dimethylformamide (DMF) is employed for the direct amidation with no such "activator" needed [44]. In addition to the methods above, other means, such as sulfonation, silylation and polymer-grafting, are also suitable for adjusting surface properties of nanocellulose. According to nanocellulose of interest, a variety of options are available to choose from.

In terms of physical modification, it is virtually less stable than chemical modification that produce covalent linkage on the surface of nanocellulose. Physical methods are representative of physical interaction, and those frequently mentioned electrostatic attraction and immobilization via hydrogen bonding belong to this domain. Since abundant hydroxyl groups of nanocellulose form intra hydrogen bonding, they can also interact with external species containing O, F and N elements with high electronegativity, leading to the association of those species with nanocellulose via hydrogen bonding. With these hydroxyl groups covered by introduced modifiers,

nanocellulose might lose its hydrophilicity, which is particularly of interest when preparing the suspension of hydrophobic nanocellulose in non-polar medium [44]. In this case, the used modifiers are designed to exhibit amphiphilicity, such as water-soluble polyethylene oxide (PEO). Polar parts form hydrogen bonding with hydrophilic functional groups of nanocellulose and non-polar parts function indeed as stabilizer to maintain the dispersion of modified nanocellulose in medium [51]. Electrostatic interaction helps in the surface modification as well. Under the condition that pretreatment is done to nanocellulose to endow it with positive and/or negative charge, the modifier with the opposite charge is capable of interacting with nanocellulose electrostatically in a desirable way [44]. It should be pointed out that physical approaches result in less stable modification compared to chemical modifications, but at the same time they have notable merits owing to their low cost and simple procedures without damaging the crystalline structure of nanocellulose. [44] In this master's project, the formation of hydrogen bonding and electrostatic attraction between TEMPO-oxidized CNF or the existing cations in CNF hydrogel and negatively charged MXene nanosheets are utilized.

1.4 Applications of nanocellulose

Nanocellulose belongs to the abundant sustainable materials having favorable and applicable properties, it can be used as such or be incorporated into other materials for better performance. Also, nanocellulose allows more possibility of processing after use thanks to its environmental friendliness, represented by its excellent biocompatibility and biodegradability. Nanocellulose has exerted itself in a wide range of applications, including energy technology, wearable electronics, and medication. As nanocellulose-based composite is fabricated for energy storage in this project, introduction to energy-device-related applications is mainly aimed at in the following sections.

Supercapacitors, carrying high power density and featuring fast charging and discharging, have been studied intensively all the time. Though nanocellulose is an insulating component, it can realize its potentials in various ways. Nanocellulose can be coupled with electroactive species as electrode materials in supercapacitor, and it also serves as a carbon source from which carbon skeleton or carbonaceous materials can be possibly derived. Besides, nanocellulose-based separator can selectively allow electrolyte ions to go through between two electrodes as well. Generally, carbon nanomaterials and conductive long-chain polymers [47], as electroactive components, are employed in many instances. By incorporating these active species, it is realistic to make a flexible composite electrode with nanocellulose as support materials, such as cellulose nanofibers and bacterial cellulose. The advantages of innate network entanglement and large aspect ratio of nanocellulose are effectively utilized for the preparation of electrode.

Carbon nanomaterials, including well-known graphene, its derivatives, and carbon nanotubes (CNT) with or without heteroatom doping, can be integrated into cellulose nanofibers to form hybrid materials. The structure and dimension of formed composites can differ drastically depending on the preparation methods. Wet spinning method brings one-dimension composite nanofibrils [47], in contrast to the fibrils in microscale obtained by mechanical process of extruding the composite dispersion. For example, Niu' group introduced CNF in order to address the issue of easy agglomeration of single-walled CNT, and further made the hybrid microfibrils with good mechanical properties via controlled extrusion [52]. They found that the assembled supercapacitor, with the prepared composite and electrolyte gel, showed remarkable cycling stability (over 95%) as well as electrochemical performance after being repeatedly twisted and bended [52]. Vacuum-assisted filtration is an advisable method when two-dimension nanocellulose-based hybrid papers or films are expected. Considering that reduced graphene oxide (rGO) has tendency to re-stack, which sacrifices its active sites and surface area when used in supercapacitor electrode, Xiong's group employed spacing

enlarger CNF into GO to fabricate flexible CNF/rGO composite electrode via vacuum filtration, subsequently followed by chemical reduction of GO towards rGO [53]. In terms of energy storage, the film performed quite well, presenting a satisfactory areal capacitance of over 100 mF/cm^2 with long-term stability [53]. Another tricky way of making two-dimension hybrid material is direct coating. Chun's group directly poured CNT dispersion on the as-prepared bacterial nanocellulose paper under continuous vacuum, instead of mixing CNT and BNC in advance before going for filtration [54].After electrochemical evaluation, they realized that the integrated supercapacitor with flexible coated BNC papers exhibited outstanding cyclability (with high capacitance retention after 5000 cycles of charging and discharging) [54]. It is noteworthy that filter used in the experiment is suggested to be compatible with the solvent in the mixture, otherwise the filter would be damaged, causing the impurities in filtered residual. Furthermore, an innovative preparation method was explored by Choi's group. It had some similarity with direct coating, but it was assisted by inkjet printing. CNF was firstly inkjetted onto normal paper as substrate, onto which some conductive materials (e.g., CNT, activated carbon and Ag nanowires) and ionic liquid-based solution were inkjet-printed with controlled pattern as electrodes and electrolyte (Figure 16), respectively [55]. This approach rendered connection of several working units much easier, which exactly was its distinct merit. Another method - freeze-drying has been reported to benefit facile preparation of three-dimension electrode materials with notable porosity. Zheng's group firstly made CNF-based composite hybridized with graphene oxide nanosheets (GONS) and CNT via freeze-drying, in which the dispersion of composite is frozen at extremely low temperature, and further went through vacuum drying to yield composite aerogel [56]. Then, they reduced the GONS existing in the hybrid towards rGO, which was finally followed by assembly and evaluation of a supercapacitor with the as-prepared composite electrodes [56]. The supercapacitor containing gel electrolyte brought extraordinary specific capacitance of over 250 F/g as well as impressive long-term stability [56]. One of the possible reasons

for its porosity was that freezing process increased the volume of water molecules in the dispersion, and therefore enlarged the separation of each domain.

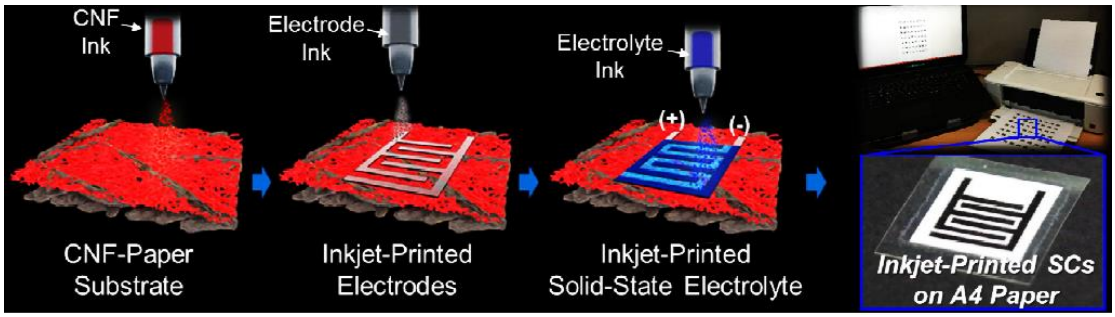

Figure 16. Schematic illustration of fabrication of nanocellulose-based supercapacitor by inkjet printing [55].

In addition to carbon nanomaterials, electroactive species can also be polymers with good electrical conductivity. PEDOT, as a conductive polymer mentioned in previous paragraph, can be incorporated into nanocellulose for energy storage. However, in many cases PSS (poly(styrene sulfonate)) couples with PEDOT to make homogeneous suspension for further fabrication composite. The use of PSS should be reduced with considerations to its availability and impact on environment [57]. To avoid the addition of PSS, Feng's group employed nanocellulose pretreated with sulfamic acid to make a highly conductive film with PEDOT, in which sulfated nanocellulose took up the role of PSS and interacted with PEDOT formed by polymerization of EDOT [57]. Likewise, Fu's group, with much ease, fabricated conductive composite film with CNF and polypyrrole by immersing CNF substrate into highly concentrated pyrrole solution, which was then followed by the polymerization of pyrrole right on CNF along with the additive (Figure 17) [58]. The supercapacitor prepared with composite films indicated satisfactory specific capacitance (over 2000 mF/cm^2 at the current density of 2 mA/cm^2) and acceptable cycling stability [58]. Furthermore, due to the low cost and facile preparation of conductive PANI, it has been wisely selected as electrode materials. PANI/CNF composite was fabricated by Zheng's group, in which they polymerized aniline on the as-prepared CNF film [59]. The obtained composite film with 40% mass loading of CNF could still display a high conductivity of nearly 180 S/cm. The composite-based supercapacitor could reach distinctive remarkable capacitance of over

400 F/g when the mass of electroactive species PANI accounted for 80% of the whole composite [59].

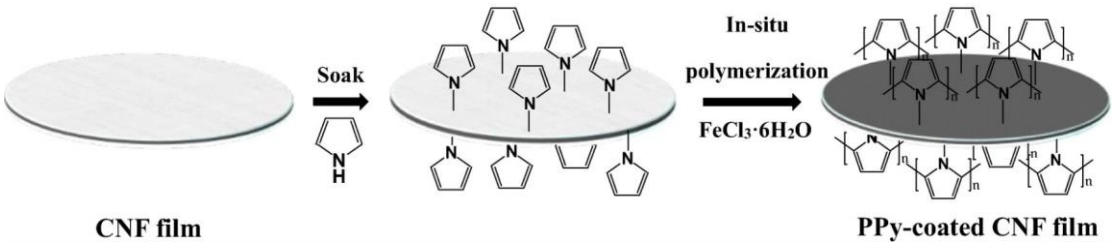

Figure 17. CNF/PPy composite made by polymerization of pyrrole on CNF [58].

Another significant application of nanocellulose lies in batteries. Compared to supercapacitors, batteries generally have higher energy density and capacity, and more stability. Research on lithium-ion batteries have been in the spotlight where strategies for development have emerged to quite a few professional battery manufacturers, such as BYD and CATL. Nanocellulose, as earth-abundant material, can be combined with electroactive species to serve as either anode or cathode in lithium-ion batteries. Because the intercalation as well as deintercalation of lithium ions at the electrodes plays a pivotal part in performance of lithium-ion batteries, the layered structure in the electrode is expected. Leijonmarck's group used CNF to interlink Super-P carbon and active species $LiFePO_4$ with semi-layered structure, which resulted in CNF-based cathode of excellent strength and stability [60]. Meanwhile, the battery built with this composite cathode exhibited outstanding capacity of 150 mAh/g at low current density, which still maintained after 10 cycles of tests [60]. A special case about lithium-ion batteries originates from a phenomenon "shuttle effect" existing in lithium-sulfur batteries, due to the dissolution of formed polysulfide into electrolyte. Nanocellulose contains abundant hydroxyl groups, therefore it can be considered to facilitate the chemisorption of newly formed species, preventing them from dissolving and enhancing the efficiency of batteries. In addition to lithium-ion batteries, sodium-ion batteries draw massive attention as well, owing to its unique potential for large-scale application. It operates in the similar way to lithium-ion batteries, which requires the movement of sodium ions within layered framework. As sodium ion owns large radius, electrode materials with increased interlayer spacing are investigated. Li's group

developed, by simply mixing two components MoS_2 and CNF together, a highly tensile composite anode for sodium battery, and its performance was indicated by a capacity of nearly 150 mAh/g with tendency to decrease with cycles [61]. Moreover, nanocellulose also benefits the ionic selectivity and permeation when it acts as separator in batteries, which is mainly attributed to its hydrophilicity. Kim's group endowed CNF with manageable porosity and thickness with the help of nanoparticle template of silica. The prepared cellulose showed less dense stacking, and functioned as separator with enhanced ionic permeation (lower IR drop) in tested lithium-ion battery when compared to its counterpart without silica [62].

1.5 The objective

In this research project, the aim is to prepare MXene/CNF self-standing composite electrodes with high conductivity and flexibility via hydrothermal treatment. $Ti_3C_2T_x$, a member of newly emerging two-dimensional materials, has high electrical conductivity while it suffers from low mechanical strength and re-stacking behavior at the same time, which severely limits its performance. For this reason, nature-abundant cellulose is introduced into MXene for improved mechanical properties, and makes possible the production of flexible MXene-based composite films. The method used for preparation is hydrothermal process, which is expected to mix two components well, and worthy of investigation since this method has not yet been reported in publication. Through hydrothermal treatment for 1 h at 80 °C under inert gas atmosphere, homogeneous dispersions of MXene/CNF composite are supposedly obtained, which are followed by fabrication of composite films by further vacuum-assisted filtration of dispersions. The dispersions are used for a series of electrochemical tests, by which the electrochemical performance can be evaluated. The obtained films go through materials characterization, by which physical and chemical properties can be assessed. The experimental procedures are well depicted in Figure 18.

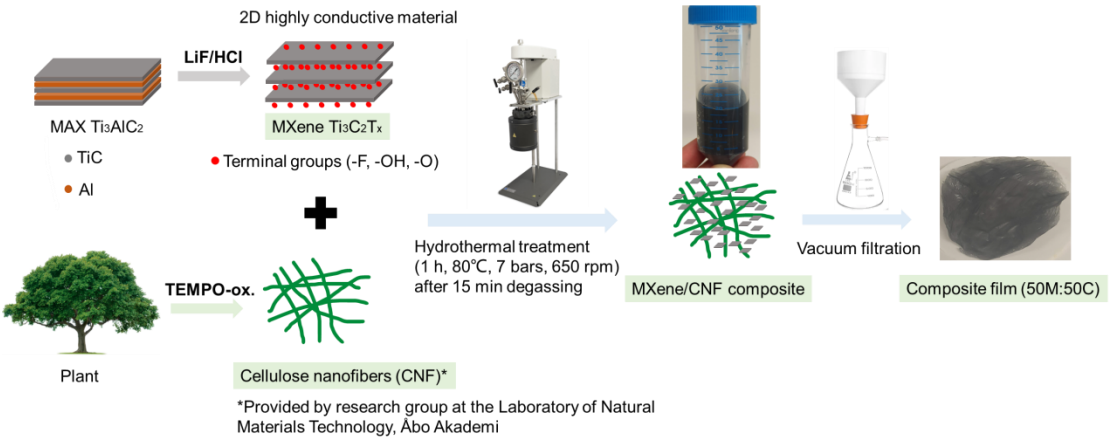

Figure 18. Schematic illustration of preparation of MXene/CNF dispersion and composite.

2 Experimental section

2.1 Materials

$Ti_3C_2T_x$ from Ashwini Jadav (UTU), Super P activated carbon powder, high-charged (HC) TEMPO-oxidized cellulose nanofiber hydrogel (0.93%), low-charged (LC) TEMPO-oxidized cellulose nanofiber hydrogel (0.88%) from Prof. Chunlin Xu & Dr. Xiaoju Wang, Åbo Akademi University, cellulose nanofiber hydrogel (1.7%) from Prof. Jaana Vapaavuori at Aalto University termed CNF Aalto, Deionized (DI) water, TiO_2 P 25 (Aeroxide), toluene, Millipore membrane filters (0.1 μm VCTP), H_2SO_4 (2.5 M, Fluka), electronic balance, Ag/AgCl electrode (previously prepared by potentiostat at potentiostatic mode), Pt wire, glassy carbon electrodes (GCE, r = 1.5 mm), Parafilm, Nafion (5%, Aldrich), n-methyl-2-pyrrolidone (NMP, 99.5%, Aldrich), graphite foils (grafoils), glass vials, Teflon lid with customized holes.

2.2 Instruments

For synthesis the following devices were used: 4848 Parr reactor, heating plate (Stuart), vacuum oven (Memmert), vacuum machine (Heto). Electrochemical studies by Autolab electrochemical station, Iviumstat potentiostat and for structural characterization the following instrumentation was used: X-ray powder diffractometer (PANalytical), Jandel four-point probe with RM3000+ test meter, FTIR spectrometer (Bruker), Raman microscope (Renishaw inVia Qontor).

2.3 Preparation of MXene/CNF composite dispersions

The dispersions with different types of cellulose at mass ratio of 10MXene:90CNF were prepared for electrochemical tests.

2.3.1 Dispersion of 10MXene:90CNF with highly-charged CNF (0.93%)

First, 10.05 mg $Ti_3C_2T_x$ and 9684.01 mg cellulose hydrogel were weighed on the electronic balance, with a small vial and a beaker as holders, respectively. Secondly, a certain amount of DI water was used to completely transfer $Ti_3C_2T_x$ into beaker containing cellulose. Thirdly, the addition of DI water was continued until the total volume of mixture in the beaker reached a mark of 20 mL, and another 5 ml of DI water was used subsequently to wash the remainings in beaker and was added to the Teflon reaction vessel. Lastly, after degassing for 15 (3×5) min, the 25 mL of mixture was treated for 1 h in a parr reactor, at a high temperature of 80 ℃ and pressure of 7 bars with 650 rpm stirring speed in inert N_2 gas atmosphere. The volume of the obtained black dispersion was measured to be 23 mL (Figure 19a).

2.3.2 Dispersion of 10MXene:90CNF with lowly-charged CNF (0.88%)

For this dispersion, 10.03 mg$Ti_3C_2T_x$ and 10240.8 mg cellulose hydrogel were weighed. The following procedures were similar to the section 2.3.1, which led to dispersion with a total volume nearly of 22 mL after hydrothermal treatment (Figure 19b).

2.3.3 Dispersion of 10MXene:90CNF with CNF Aalto (very high-charge) CNF (1.7%)

For this dispersion, 10.0 mg $Ti_3C_2T_x$ and 5297.1 mg cellulose hydrogel were weighed. The following procedures were similar to the section 2.3.1 as well, which led to dispersion with a total volume nearly of 22 mL after hydrothermal process (Figure 19c).

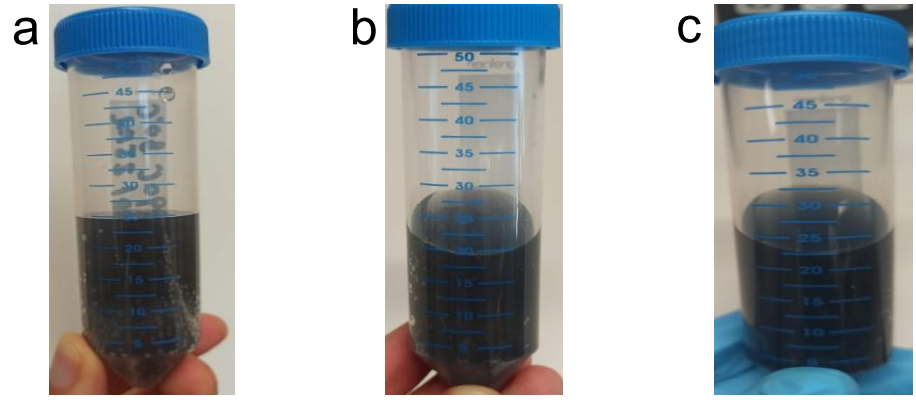

Figure 19. Different dispersions of MXene/CNF obtained after hydrothermal treatment.

2.4 Preparation of MXene/CNF composite films

The composite films with highly-charged CNF (0.93%) at different mass ratios of 10MXene:90CNF, 50MXene:50CNF and 70MXene:30CNF were prepared by vacuum-assisted filtration of corresponding dispersions. These films were analyzed by materials characterization techniques.

Preparation of 10MXene90CNF film

10 mL of previously made 10MXene:90CNF dispersion was taken out and slowly dropped onto a hydrophilic filter membrane placed in funnel under continuous vacuum condition, followed by drying overnight. After drying, the semi-transparent bendable film 10MXene90CNF hydro (Figure 20) was collected for further physical characterizations.

Preparation of 50MXene50CNF film

For this film, fresh dispersion at a mass ratio of 50MXene:50CNF was required in advance. 11.98 mg $Ti_3C_2T_x$ and 1288.84 mg cellulose hydrogel were weighed, mixed to a total volume of 12 mL and treated hydrothermally under the same conditions mentioned in the section 2.3.1. The finally obtained dispersion had a volume of almost 10 mL. Similarly, it was dropped onto a filter membrane to fabricate a film 50MXene50CNF hydro (Figure 20), which appeared black with a certain degree of flexibility.

Preparation of 50MXene50CNF film pretreated by sonication

This 50MXene50CNF sonic film was prepared, for comparison, in a different way by Mr. Yu Zou in the same research group. The main difference was that after $Ti_3C_2T_x$ and cellulose were separately pre-sonicated for 15 min, a mixture of $Ti_3C_2T_x$ and cellulose was sonicated for another 1 h at room temperature. The mixture then went through the same filtration, which resulted in a composite film.

Preparation of 50MXene50CNF film prepared with toluene

This film was prepared in water-free toluene medium for comparison with film prepared in DI water. 11.7 mg $Ti_3C_2T_x$ and 1243.78 mg cellulose hydrogel were weighed, which were then mixed with the use of toluene to a total volume of 12 mL and processed hydrothermally under the same conditions stated in the section 2.3.1. Due to the hydrophobicity and volatility of toluene, a film was directly formed and remained in the reaction vessel after hydrothermal treatment.

Preparation of 50$TiO_2$50CNF film

This film was prepared for comparison, by replacing $Ti_3C_2T_x$ with TiO_2. 11.9 mg TiO_2 and 1281.8 mg cellulose were weighed, and processed in DI water in the same way as that for mixture of $Ti_3C_2T_x$ and cellulose in the section 2.3.1. The obtained dispersion had a total volume of 7.5 mL, which was filtered to yield a white fragile film.

Preparation of 70MXene30CNF film

For this film, dispersion at a mass ratio of 70MXene:30CNF was required as well. 12.01 mg $Ti_3C_2T_x$ and 552.0 mg cellulose hydrogel were weighted, mixed and treated hydrothermally under the same conditions in the section 2.3.1. 10 mL dispersion was obtained and filtered on a membrane, which led to a black film 70MXene30CNF hydro with cracks (Figure 20).

Figure 20. Dried composite films after vacuum-assisted filtration.

Preparation of cellulose film

The pure cellulose film was prepared for comparison in materials characterization. 1160.1 mg HC CNF (0.93%) was weighed, and DI water was added in dropwise to reach a volume of 10 mL. Afterwards, another 5 mL DI water transferred cellulose into reaction vessel. The cellulose solution was treated in the same hydrothermal way as composites in the section 2.3.1, which led to a volume of 12 mL, and subsequently a transparent film after vacuum filtration.

Preparation of cellulose film pretreated by sonication

This film was prepared by Mr. Yu Zou, and helped to complement data for comparison in material characterization. 1186.74 mg HC CNF was weighed and sonicated at room temperature for 75 min, which resulted in a film after filtration.

2.5 Electrochemical measurements

Cyclic voltammetric (CV) tests of conductive carbon

The CV tests with activated carbon were conducted in order to find the optimal areal density that should be applied on electrode when tested with $Ti_3C_2T_x$. 3.0 mg activated carbon powder and 200µl ethanol as solvent were mixed, and sonicated for 30 min at room temperature, which was expected to disperse carbon in solvent homogeneously. The parafilm was used to seal the dispersion to mitigate the loss of solvent due to volatilization. Different volumes of dispersion containing 0.07 mg (indicating areal density of 1 mg/cm^2 on GCE), 0.14 mg (2 mg/cm^2), 0.28 mg (4 mg/cm^2) and 0.56 mg (8 mg/cm^2) of activated carbon together with 1 µl Nafion (5%) binder were drop-cast onto one GCE for each test, separately. Thereafter the sample was dried with a drying lamp, the loaded GCE (as working electrode) and another unloaded GCE (as both counter and reference electrodes), forming two-electrode system in an assembled electrochemical cell, were immersed in 1 M H_2SO_4 electrolyte, and ready for CV tests within the potential range of 0 ~ 1 V at different scan rates of 5 mV/s, 10 mV/s, 50 mV/s and 100 mV/s. In addition, two unloaded GCEs were tested by CV under the same conditions for comparison.

Cyclic voltammetric (CV) tests of MXene/CNF composites with GCE

Composites made with three types of CNF (containing 0.14 mg $Ti_3C_2T_x$) were separately drop-cast onto one GCE (with an area of 0.07 cm^2) to reach the optimal MXene areal density (2 mg/cm^2), and dried with drying lamp, which was followed by the addition of Nafion (5%) based on the mass ratio of MXene:Nafion 2:1. After being fully dried, the composite-loaded GCE (as working electrode) was immersed in 1 M H_2SO_4 electrolyte, together with Ag/AgCl electrode (as reference electrode) and coiled Pt wire (as counter electrode), to form three-electrode system. After degassing with N_2 gas for 15 min, the CV tests were conducted within the potential range of -1 ~ 1 V at a selected scan rate of 50 mV/s for several cycles until it was stabilized.

Cyclic voltammetric (CV) tests of MXene/CNF composites with graphite foils

With considerations to long-time drop-casting caused by high content of water in 10MXene90CNF dispersions of three types of CNF, 10 mL (4 mg $Ti_3C_2T_x$) of each dispersion was firstly distributed equally in two centrifuge tubes for freeze-drying for 4 h, with the help of liquid nitrogen, to reduce the volume (down to 2 ~ 3 mL for each tube) and water content. Secondly, two sets of mixture together with the added 10 µl NMP in two tubes were drop-cast onto the end area of 1 cm^2 of two symmetrical graphite foils with the optimal MXene areal density (2 mg/cm^2), and dried by drying lamp. Thirdly, 11µl Nafion (5%) binder was added separately on two grafoils based on mass ratio of MXene:Nafion 2:1 before the composites fully dried. Finally, after drying, Teflon tape was used to cover the upper and back area of grafoils to eliminate its effect on electrochemical performance when grafoils were immersed in electrolyte. Two loaded grafoils (Figure 21a), forming two-electrode system in a designed electrochemical cell (Figure 21b), were immersed in 1 M H_2SO_4, and ready for CV tests within the potential range of 0 ~1 V at different scan rates of 5 mV/s, 10 mV/s, 50 mV/s and 100 mV/s. In addition, MXene-loaded grafoils and unloaded grafoils were tested by CV tests for comparison.

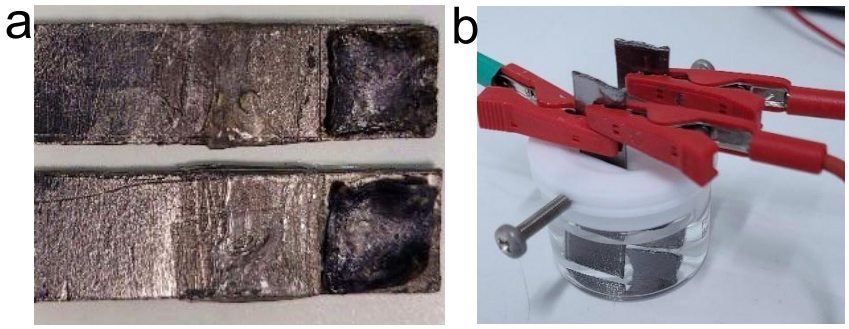

Figure 21. (a) Composites-loaded graphite foils; (b) Assembled electrochemical cell for CV test.

Electrochemical impedance spectroscopic (EIS) tests of MXene/CNF composites

For EIS tests, the same electrochemical cell with 10MXene90CNF composite-loaded grafoils was used in order to understand the electrochemical behavior of 10MXene90CNF composites (at the interface between electrode and electrolyte) in more detail. The EIS tests were conducted at a low amplitude of 0.1 V within a frequency range of 0.1 Hz ~ 100 kHz. In addition, MXene-loaded grafoils were also analyzed by EIS test for comparison.

Galvanostatic charging discharging (GCD) tests of MXene/CNF composites

For GCD tests, the same electrochemical cell containing 10MXene90CNF composite-loaded grafoils was used right after it completed CV and EIS tests of different composites each time. The GCD tests were conducted within voltage range of 0 ~ 1 V for total 1000 cycles of charging and discharging with each 100th cycle recorded, at different applied current densities of 1 mA/cm^2, 2 mA/cm^2, 5 mA/cm^2 and 10 mA/cm^2. In addition, MXene-loaded grafoils were tested as well for comparison. Areal capacitances for symmetric supercapacitor system were calculated based on discharging time and voltage provided by GCD tests, the equation of which is shown in the following:

$$Areal\ capacitance_s = \frac{2 \times I_a \times \Delta t}{(\Delta V - IR)} = \frac{2 \times I_a \times \Delta t}{\Delta V_r}$$

In this equation, I_a refers to the current density applied in areal unit; IR refers to the voltage drop due to internal resistance in the system, which is deducted to give real discharging voltage; Δt refers to the discharging time. Based on the calculated areal capacitances, capacitance retentions after each 100 cycles for a composite were compared.

2.6 Materials characterization

Conductance tests

The resistance of composite films with different mass ratios of MXene and CNF (10MXene90CNF hydro, 50MXene50CNF hydro, 50MXene50CNF sonic, 70MXene30CNF hydro) was measured with linear-array 4-point test meter. Prior to measurement, calibration was done. A small size grafoil sample was placed beneath four probes, and tightened by adjusting properly the screw affiliated to the probes, followed by I-V characterization with the set voltage range of -0.4 ~ 0.4 V, and subsequent observation that I-V curve passed the origin point. Then, resistance of these four composite films were measured in the same way as grafoil. Finally, resistance was converted to conductance, which was the reciprocal resistance.

X-ray powder diffraction (XRD) analyses

X-ray diffractometer was used to analyze composite films (50MXene50CNF hydro, 50MXene50CNF sonic), cellulose films and MXene powder. Silicon substrate was selected due to its “zero” background, which exhibited limited interference with samples. The samples were scanned by Cu Kα source at “fast scan” mode.

Fourier-transform infrared spectroscopy (FT-IR) analyses

FT-IR spectrometer was used to analyze composite films (50MXene50CNF hydro, 50MXene50CNF sonic) and cellulose films. Measurement on background was done in advance of films, which was automatically subtracted in original spectra of films. Different sites on each sample were scanned at ATR mode to ensure that the spectra were repeatable.

Raman analyses

Raman microscope was used to analyze composite films (50MXene50CNF hydro, 50MXene50CNF sonic, 50MXene50CNF-toluene, 50$TiO_2$50CNF). Different sites on each sample were scanned with a 532 nm laser of 5% power.

3 Results and discussion

3.1 Electrochemical performance

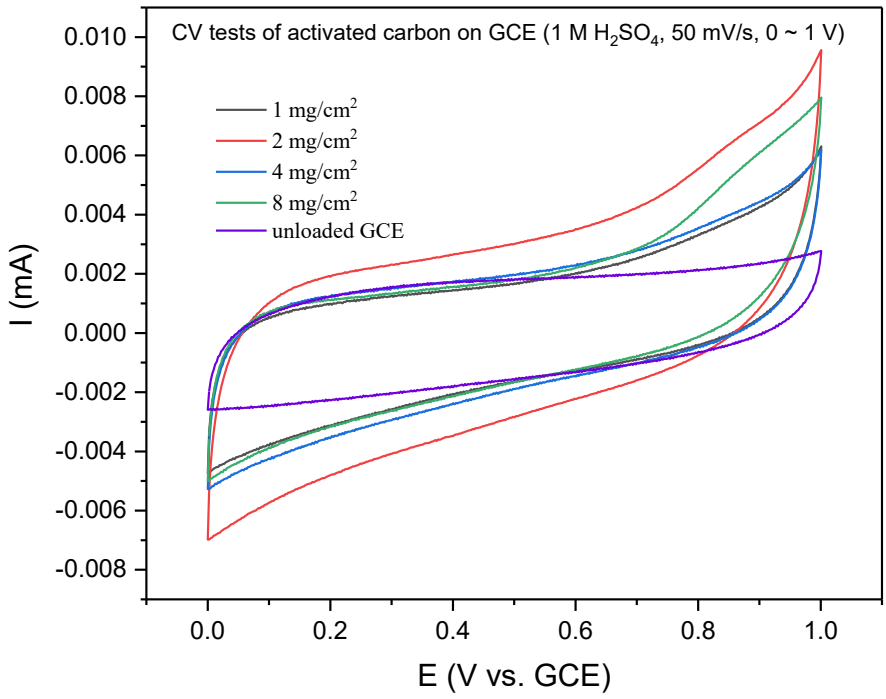

Figure 22. CV tests of activated carbon on GCE in two-GCE system within the potential range of 0 ~ 1 V at a scan rate of 50 mV/s.

Activated carbon was employed to estimate the possible proper amount of MXene that should be loaded on electrode. The current response of conductive carbon with different areal density on GCE was measured by CV, which is shown in Figure 22. It is clearly seen that the activated carbon with an areal density of 2 mg/cm^2 exhibits highest current response among all the four areal contents. Interestingly, current decreases with increasing mass loading of carbon, which likely derives from the loss of electroactive sites due to the unnecessary addition.

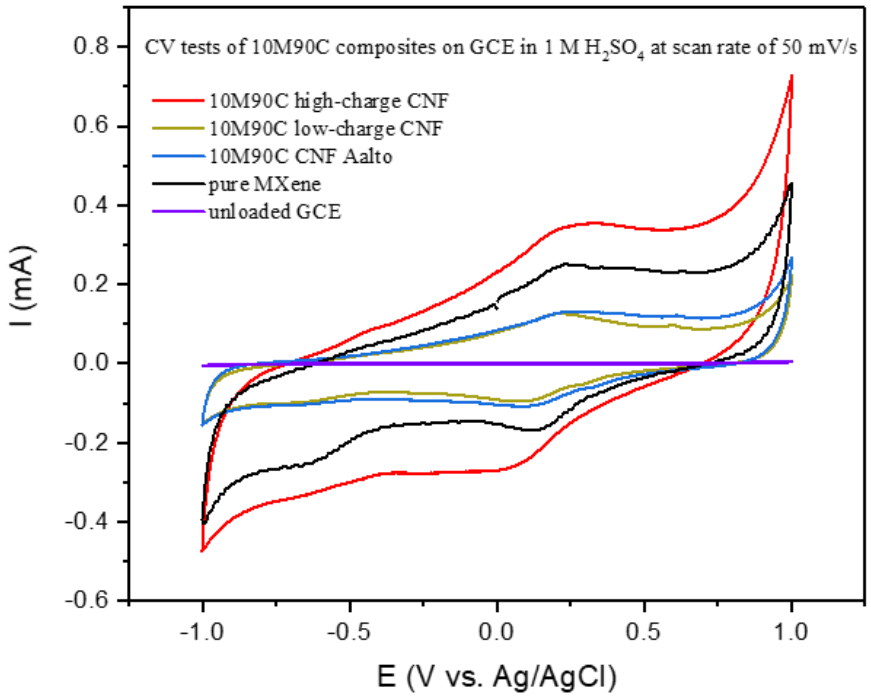

Figure 23. CV tests of 10MXene90CNF (10M90C) composites different CNF on GCE in three-electrode system within the potential range of -1 ~ 1 V at a scan rate of 50 mV/s.

Electrochemical activity of 10MXene90CNF composite containing three different CNF was then simply measured by CV in a broader potential range of -1 ~ 1 V (Figure 23). With the possible optimal MXene areal density of 2 mg/cm^2 applied, composite of high-charge CNF exhibits highest current response with most broad current range appearing in its CV loop, while lower current is observed for composites of other two CNF. Compared to pure MXene, the current (CV area) of composite with high-charge CNF is increased notably, and then reverse for other CNF, from which it can be inferred that the introduction of high-charge CNF increases the electroactivity of MXene on GCE while other two CNF hinders its performance. It may be explained by high degree of TEMPO oxidation in high-charge CNF, which endows it with large concentration of charge-containing carboxylate ions, and renders it easier to mix uniformly with MXene. Meanwhile, it is noteworthy that all the composites as well as pure MXene show redox peaks in the middle of smooth curves between 0 and 0.25 V. This observation indicates

that faradaic current is generated from redox reactions at certain potentials, in addition to capacitive current of smooth parts.

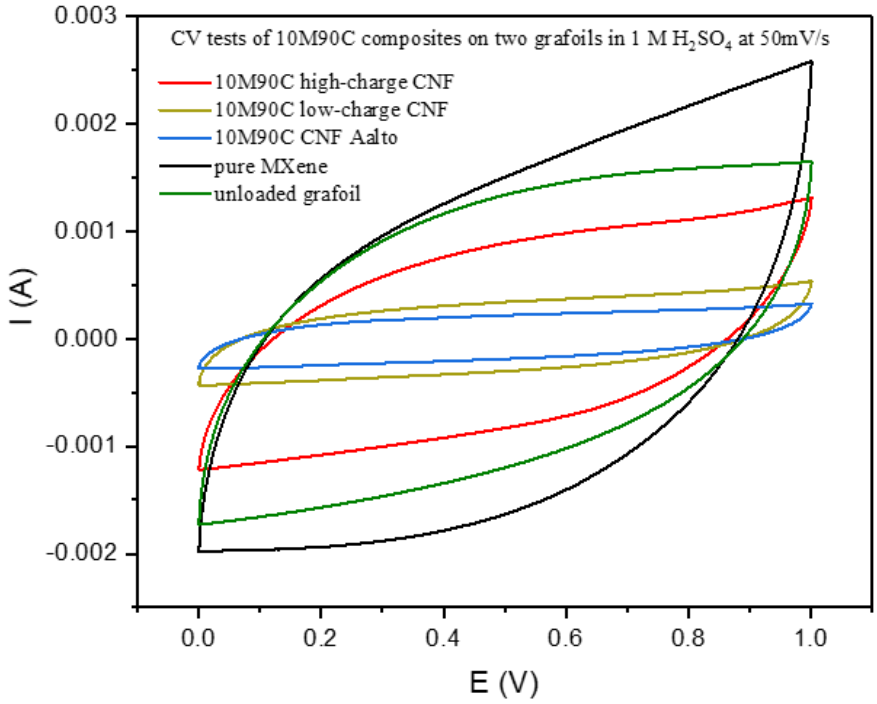

Figure 24. CV tests of 10MXene90CNF (10M90C) composites of different CNF loaded equally on two grafoils within the potential range of 0 ~ 1 V at a scan rate of 50 mV/s.

To mimic a supercapacitor, two grafoils with the same loading of composites were placed oppositely in electrolyte and fixed by screws at two sides, as shown in Figure 21. The electrochemical performance of this two-electrode system was analyzed by CV as well (Figure 24), but with a selected potential range of 0 ~ 1 V for faster measurement. Similarly, composite of high-charge CNF displays highest current response among all the composites. However, its current is obviously lower than that of pure MXene, and even unloaded grafoils. This remarkable inconsistency with GCE-assisted tests might derive from the increasing loading of the insulating species cellulose on bigger area on grafoils, which further worsens MXene's electrochemical performance.

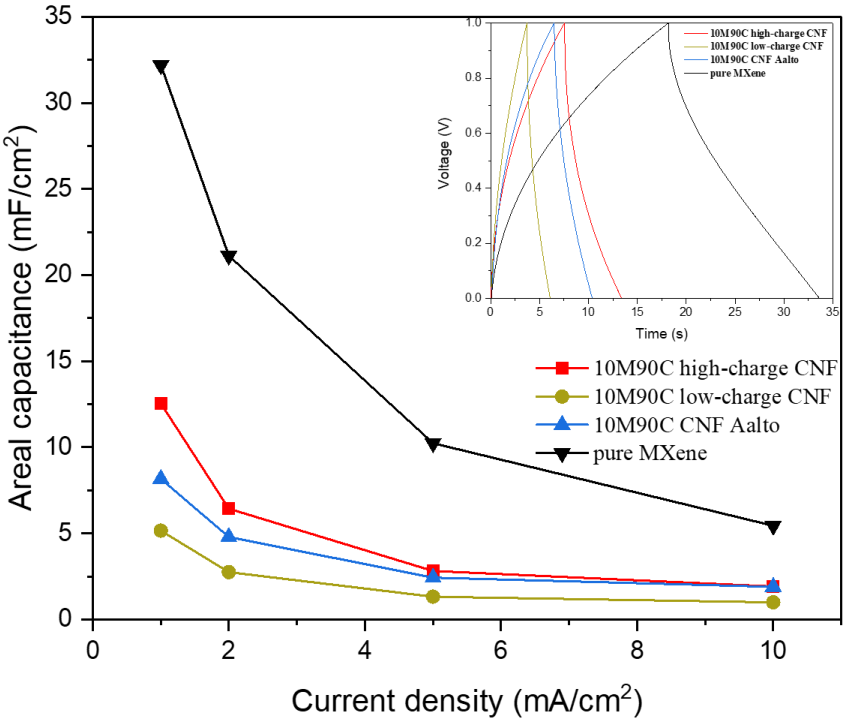

Figure 25. Areal capacitances of 10MXene90CNF (10M90C) composites of different CNF at different current densities. Inset: GCD plots of composites within the voltage range of 0 ~ 1 V in 1 M H_2SO_4 at applied current density of 1 mA/cm^2.

Afterwards, GCD tests were applied on the same electrochemical cell containing 10MXene90CNF composite-loaded grafoils. In the inset (Figure 25), it can be seen at current density of 1 mA/cm^2, pure MXene has the longest discharging time of ca. 15 s, followed by the composites of high-charge CNF, CNF Aalto and low-charge CNF in decreasing order of capacitance. Using the equation stated in Experimental section, areal capacitances at different applied current densities can be obtained. The composite of high-charge CNF gives the highest areal capacitance of 12.5 mF/cm^2 at 1 mA/cm^2, almost doubling the capacitance of low-charge CNF composite (5.2 mF/cm^2), among all the composites, and areal capacitances for these three composites experience step-down with increasing current applied, leading to a notable decrease to areal capacitances of below 2 mF/cm^2 for all the prepared composites at 10 mA/cm^2. In accordance with expectations, pure MXene dominates with an impressive areal

capacitance of 32.2 mF/cm^2 at 1 mA/cm^2 and continues to be highest at increasing current densities, which also corresponds to the results in CV analyses.

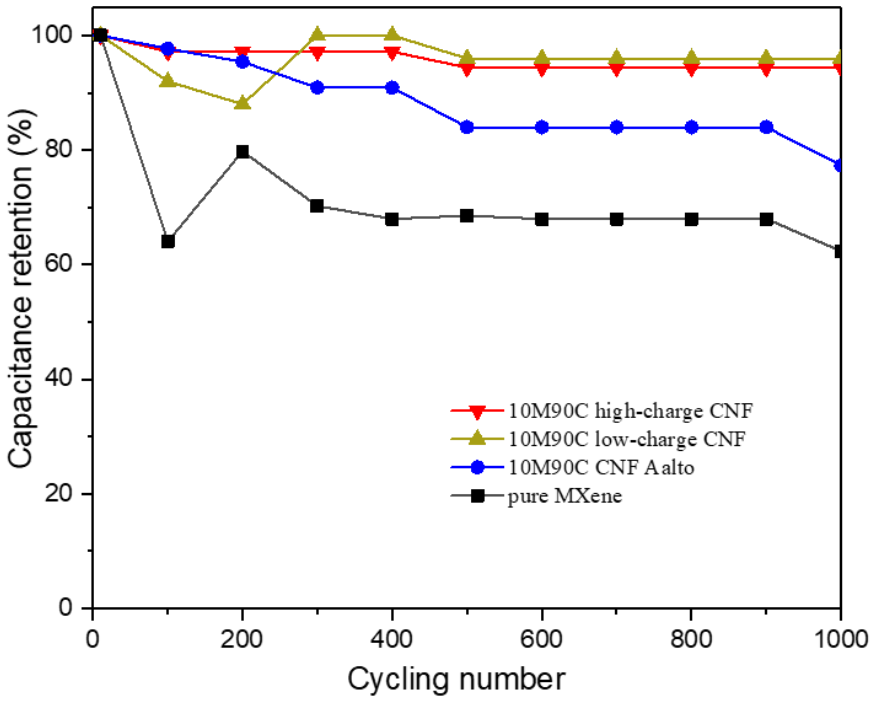

Figure 26. Capacitance retention of 10MXene90CNF (10M90C) composites of different CNF within the voltage range of 0 ~ 1 V in 1 M H_2SO_4 at 10 mA/cm^2 with increasing cycling number.

When it comes to cycling stability, composites behave distinctly better than pure MXene. Over 1000 cycles of charging and discharging, all the composites maintain relatively high capacitance retentions of over 80%, especially for high-charge CNF and low-charge CNF composites (beyond 90%) with a steady decrement, while the capacitance retention of pure MXene declines to around 60% after a dramatic decrease over the first 100 cycles (Figure 26). It implies that the incorporation of cellulose improves long-term stability of MXene.

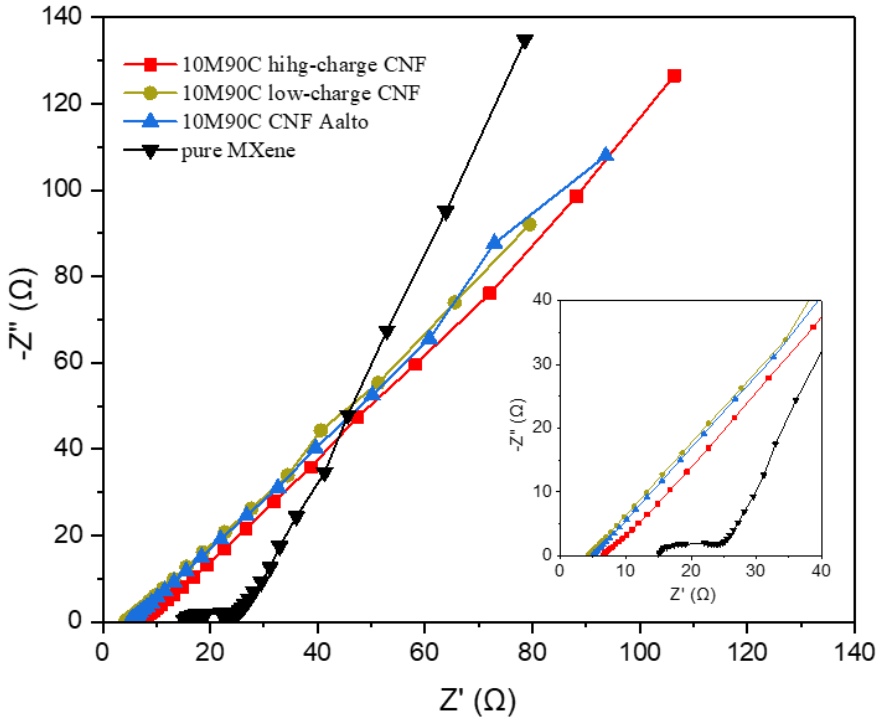

Figure 27. Nyquist plot from EIS tests of 10MXene90CNF (10M90C) composites of different CNF in 1 M H_2SO_4 at frequency range from 0.1 Hz to 100kHz.

In the Nyquist plot, there is no semi-circle, representing the charge transfer resistance, observed for composites, but with typical lines of nearly 45° phase angle throughout the entire range of frequency (Figure 27), which indicates that diffusion process at the interface between electrode and electrolyte is the rate-determining step, and therefore controls the impedance of composites. As for pure MXene, it is analyzed to exhibit more pronounced capacitive behavior owing to the bigger slope in the low-frequency region. The impedance of pure MXene indicates a mixed kinetic and diffusion control as a semi-circle, representing a charge transfer resistance of 10Ω, is observed in the plot.

Based on these electrochemical analyses, it can be concluded that the introduction of cellulose nanofibers might deteriorate electrochemical performance of MXene, but compensates the loss by enhancing its stability. Among three kinds of CNF, high-

charge CNF works best for composite. Thereafter, high-charge CNF was selected for preparation of composite films.

3.2 Materials characterization

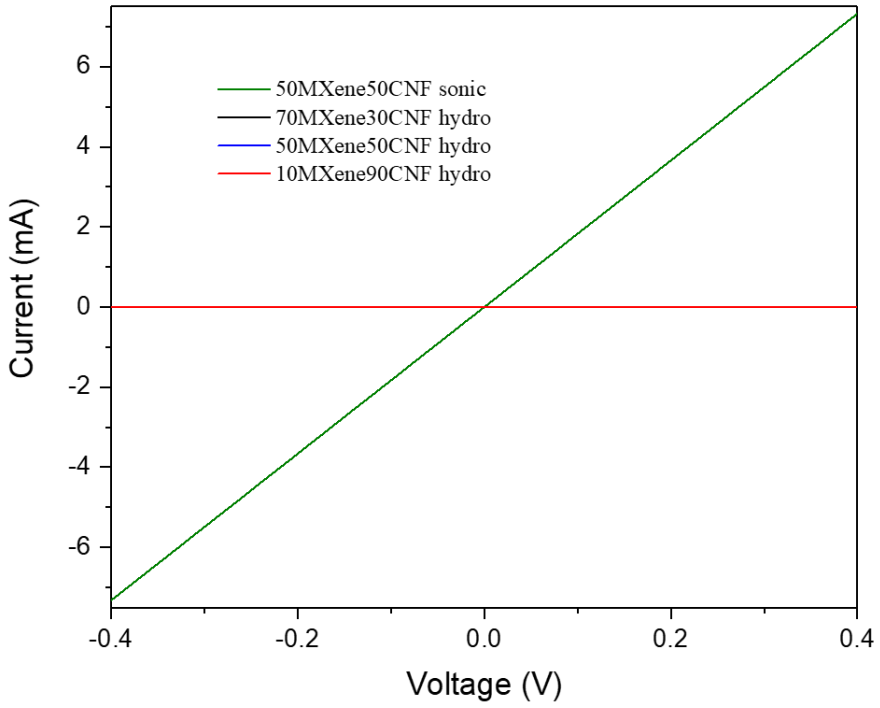

Figure 28. I-V plot from conductance tests of composite films with different mass ratios and pretreatment methods.

Since MXene/CNF composites are expected to act as self-standing electrodes, high-charge CNF composite films with different mass ratios of MXene and cellulose were fabricated in a hydrothermal way, which enables investigation into their properties as electrodes. In Figure 28, I-V curves of hydrothermally pretreated composites are represented by three overlapped horizontal lines, which clearly demonstrate poor electric conductance of composites no matter what mass percentage conductive MXene accounts for. To the contrast, composite pretreated by sonication yields a distinguished conductance of ca.0.018 S derived from current of 7 mA at 0.4 V, which is over 200 ~

700 times larger than conductance of hydrothermal composites. Thus, it is reasonable to look more into their difference to unveil the underlying cause that might have something to do with the preparation methods. Because 50MXene50CNF hydro and 50MXene50CNF sonic composites differ apparently from each other in terms of conductance, these two composite films were selected for further analyses.

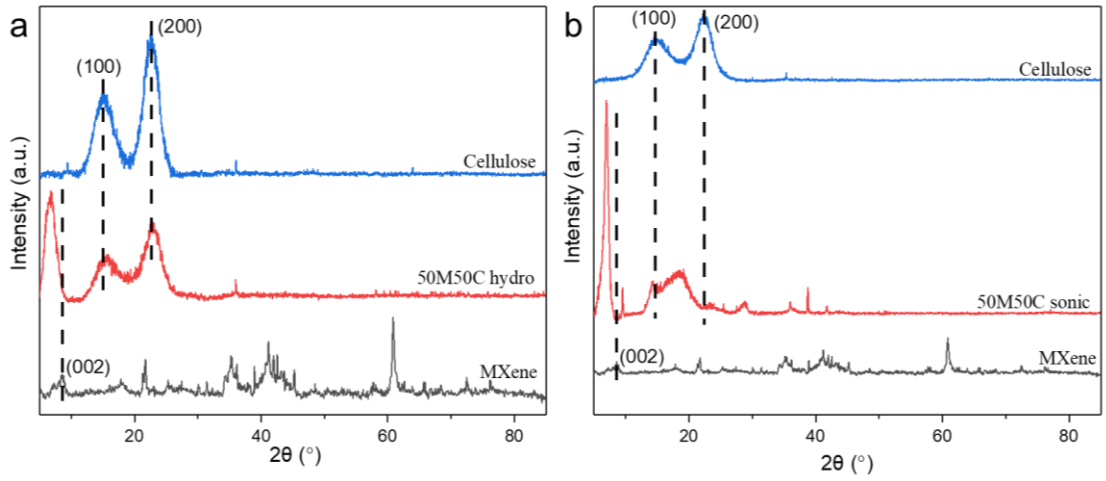

Figure 29. XRD patterns of 50MXene50CNF (50M50C) composites pretreated differently in comparison to pure MXene powder and cellulose films.

The crystallographic structure of two 50MXene50CNF composites were analyzed and compared by XRD (Figure 29). In case of 50MXene50CNF hydro composite film, the characteristic peak of MXene at diffraction angle of 8.6°, referring to the (002) crystal plane, shifts to a lower angle of 6.8° after being processed with cellulose, which implies that d-spacing of MXene is enlarged. Moreover, two typical peaks, attributed to the (100) and (200) crystal plane of cellulose I crystal structure, are observed in hydro composite as well. It proves that CNF is successfully introduced into MXene. The increased distance between nanosheets in hydro composite can possibly be explained by the intercalation of CNF and hydrothermal process. With regards to 50M50C sonic composite film, similar peak shift from MXene can be seen, while some structural change might have occurred to cellulose in sonic composite as the peaks from cellulose left-shift and become slightly broader.

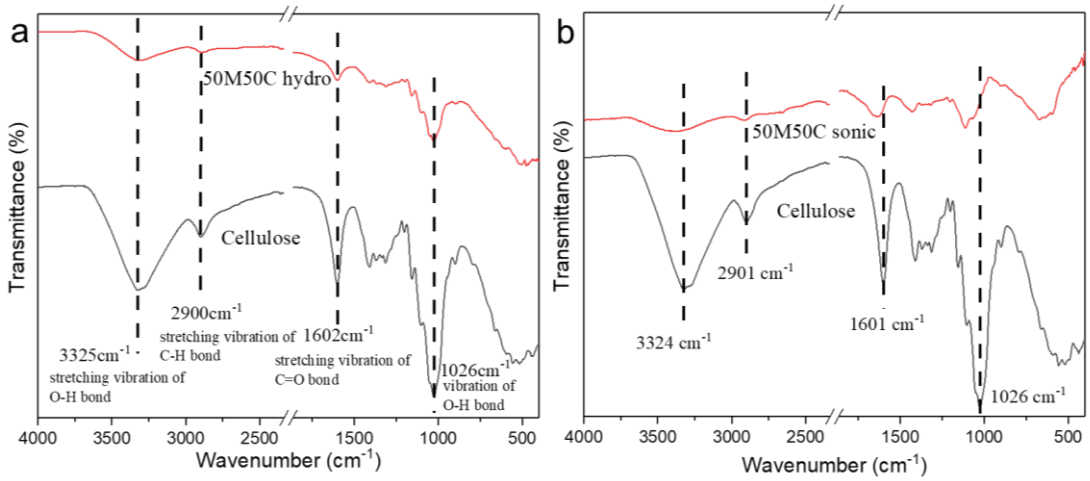

Figure 30. FT-IR spectra of50MXene50CNF (50M50C) composites pretreated differently in comparison to cellulose films.

FT-IR helps to unravel bonding within the composite materials. In the spectra, vibrations of O-H bond, C-H bond, C=O bond and O-H bond in CNF are represented by absorption peaks at four wavenumbers of 3324 cm^{-1}, 2901 cm^{-1}, 1601 cm^{-1} and 1026 cm^{-1}, respectively (Figure 30). Compared to cellulose film, 50M50C hydro composite film shows almost no peak shift from these four major absorption peaks, but 50M50C sonic composite film exhibits broader peaks, accompanied by blue shift towards higher wavenumber. The reason behind this visible shift might be that sonication process breaks hydrogen bonding within cellulose matrix, and MXene sheets get in between cellulose nanofibers displaying poor interaction with CNF, while hydrothermal treatment causes limited damage to hydrogen bonding, so there is no peak shift. This also corresponds to the peak shift from cellulose in sonic composite in XRD analyses, indicating the stronger separation between CNF after sonication. Therefore, it can be inferred that sonication disperses CNF and MXene better than hydrothermal method.

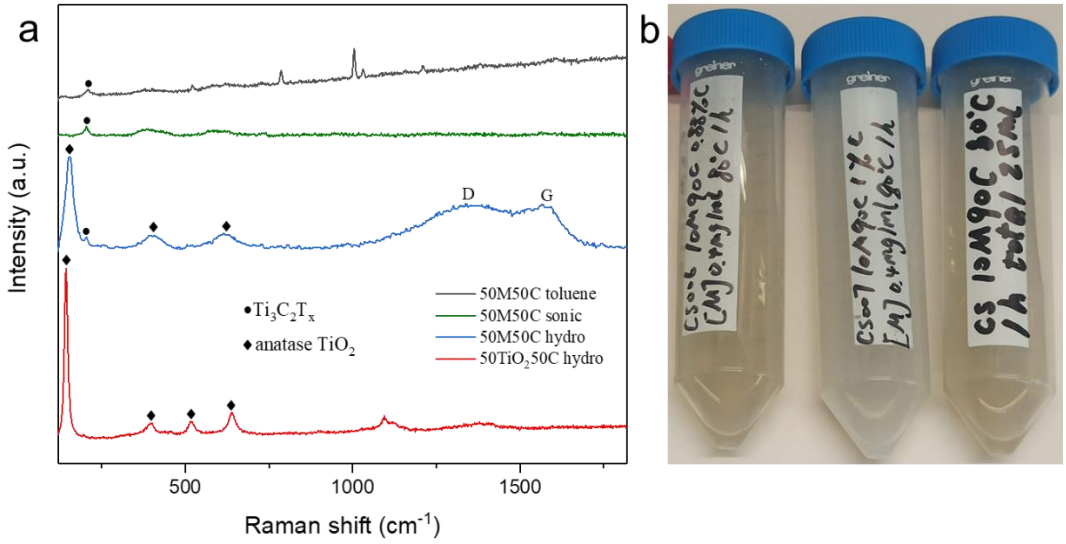

Figure 31. (a) Raman spectra of 50MXene50CNF (50M50C) composite films in comparison to toluene-pretreated film and TiO_2-based film 50$TiO_2$50CNF (50$TiO_2$50C); (b) Composite dispersions after being placed for over a month.

Raman spectra complement information about the materials. As MXene-based composite was suspected to oxidize during hydrothermal treatment, organic solvent toluene was then selected to create a water-free medium for the process. In Figure 31a, the peaks at 206 cm^{-1}, corresponding to the existence of $Ti_3C_2T_x$ phase, are observed distinctly in both toluene-pretreated and sonic composites. In addition, in case of 50MXene50CNF-toluene film, the peaks at 786 cm^{-1}, 1004 cm^{-1}, 1030 cm^{-1} and 1210 cm^{-1} are believed to derive from toluene left in the composite. After hydrothermal process, the obtained hydro composite exhibits three evident peaks at 155cm^{-1}, 397 cm^{-1} and 627 cm^{-1}, which are identified to be ascribed to the formation of the anatase TiO_2 by comparison to TiO_2-based composite. Meanwhile, two broad peaks from the D and G bands of graphitic carbon as well as a minor peak from $Ti_3C_2T_x$ are observed as well. These results indicate that $Ti_3C_2T_x$ is oxidized during hydrothermal process towards TiO_2 to a certain extent, bringing the formation of graphitic carbon, while sonication renders $Ti_3C_2T_x$ almost unchanged. It also sheds light on the phenomenon that composite dispersions experienced color change from black to opaque white over a month (Figure 31b), which might result from the oxidation of $Ti_3C_2T_x$.

4 Conclusion and prospects

According to the experimental analyses, the incorporation of cellulose nanofibers into MXene leads to a decrease in electric conductivity as well as capacitance, but benefits the composite in a way of endowing it with film flexibility and enhanced cycling stability. Specially, high-charge CNF composite exhibits a high capacitance retention of over 95% after 1000 cycles of charging and discharging, and its film with proper mass ratio of MXene and CNF shows great bendability. The limited conductivity and capacitance might likely be a consequence of oxidation of MXene in hydrothermal process. Moreover, hydrothermal method might not be good for preparing $Ti_3C_2T_x$-based composites as $Ti_3C_2T_x$ tends to oxidize in water, especially at high temperature, and CNF and MXene are not well dispersed. To the contrast, sonication is a better way of synthesizing MXene/CNF composite.

Since MXenes are a large group of materials with diverse properties, they hold promising prospects in a number of applications. With respect to this research project, other preparation methods can be considered, such as dip-coating and sonication, as mentioned and used already. For the purpose of achieving high electrical conductivity and excellent mechanical properties of MXene-based composites, surface modification (e.g., controlled terminal replacement on MXene) and/or introduction of other conductive polymers (e.g., PPy, PEDOT) may be feasible. In all, MXenes have full potential to serve as frontier materials in both academia and industry in the future.

References

[1] Poonam, Sharma Kriti, Arora Anmol, Tripathi, S.K., Review of supercapacitors: Materials and devices, Journal of Energy Storage, 2019, 21, 801-825.

[2] Kalam Amir Abul, Park Soobin, Seo Yongho, Bae Joonho. High-efficiency supercapacitor electrodes of CVD-grown graphenes hybridized with multiwalled carbon nanotubes, Bull. Korean Chem. Soc., 2015, 36 (8), 2111–2115.

[3] Zheng Ling, Chang E. Ren, Meng-Qiang Zhao, Jian Yang, James M. Giammarco, Jieshan Qiu, Michel W. Barsoum, Yury Gogotsi. Flexible and conductive MXene films and nanocomposites with high capacitance, PNAS, 2014, 111 (47), 16676-16681.

[4] Dongning Liu, Yujiao Gao, Yiheng Song, Hengfeng Zhu, Linjun Zhang, Yuanyuan Xie, Hui Shi, Zhuqun Shi, Quanling Yang, Chuanxi Xiong. Highly sensitive multifunctional electronic skin based on nanocellulose/MXene composite films with good electromagnetic shielding biocompatible antibacterial properties, Biomacromolecules, 2022, 23 (1), 182-195.

[5] Xiaohua Li, Feitian Ran, Fan Yang, Jun Long, Lu Shao. Advances in MXene films: synthesis, assembly, and applications, Trans. Tianjin Univ., 2021, 27 (3), 217–247.

[6] Babak Anasori, Yury Gogotsi. MXenes: trends, growth, and future directions. Graphene and 2D Mater., 2022, 7, 75–79.

[7] Michael Naguib, Murat Kurtoglu, Volker Presser, Jun Lu, Junjie Niu, Min Heon, Lars Hultman, Yury Gogotsi, Michel W. Barsoum. Two-dimensional nanocrystals produced by exfoliation of Ti_3AlC_2, Adv. Mater., 2011, 23 (37), 4248–4253.

[8] Aihu Feng, Yun Yu, Yong Wang, Feng Jiang, Yang Yu, Le Mi, Lixin Song. Two-dimensional MXene Ti_3C_2 produced by exfoliation of Ti_3AlC_2, Materials & Design, 2017, 114, 161-166.

[9] Patrick Urbankowski, Babak Anasori, Taron Makaryan, Dequan Er, Sankalp Kota, Patrick L. Walsh, Mengqiang Zhao, Vivek B. Shenoy, Michel W. Barsouma,

Yury Gogotsi. Synthesis of two-dimensional titanium nitride Ti_4N_3 (MXene), Nanoscale, 2016, 8, 11385-11391.

[10] Tengfei Li, Lulu Yao, Qinglei Liu, Jiajun Gu, Ruichun Luo, Jinghan Li, Xudong Yan, Weiqiang Wang, Pan Liu, Bin Chen, Wang Zhang, Waseem Abbas, Raheela Naz, Di Zhang. Fluorine-free synthesis of high-purity $Ti_3C_2T_x$ (T=OH, O) via alkali treatment, Angew. Chemie, 2018, 57 (21), 6115-6119.

[11] Chuan Xu, Libin Wang, Zhibo Liu, Long Chen, Jingkun Guo, Ning Kang, Xiu-Liang Ma, Hui-Ming Cheng, Wencai Ren. Large-area high-quality 2D ultrathin Mo_2C superconducting crystals, Nature Materials, 2015, 14 (11), 1135-1141.

[12] Rodrigo Mantovani Ronchi, Jeverson Teodoro Arantes, Sydney Ferreira Santos. Synthesis, structure, properties and applications of MXenes: Current status and perspectives, Ceramics International, 2019, 45 (15), 18167-18188.

[13] Jizhen Zhang, Na Kong, Simge Uzun, Ariana Levitt, Shayan Seyedin, Peter A. Lynch, Si Qin, Meikang Han, Wenrong Yang, Jingquan Liu, Xungai Wang, Yury Gogotsi, Joselito M. Razal. Scalable manufacturing of free-standing, strong $Ti_3C_2T_x$ MXene films with outstanding conductivity, Adv. Mater., 2020, 32 (23), 2001093.

[14] Xiao Tang, Xin Guo, Wenjian Wu, Guoxiu Wang. 2D metal carbides and nitrides (MXenes) as high-performance electrode materials for lithium-based batteries, Adv. Energy Mater., 2018, 8 (33), 1801897.

[15] Babak Anasori, Yury Gogotsi. Introduction to 2D transition metal carbides and nitrides (MXenes), In: Anasori, B., Gogotsi, Y. (eds) 2D Metal Carbides and Nitrides (MXenes), Springer, Cham., 2019, 3–12.

[16] Maria R. Lukatskaya, Olha Mashtalir, Chang E. Ren, Yohan Dall'Agnese, Patrick Rozier, Pierre-Louis Taberna, Michael Naguib, Patrice Simon, Michel W. Barsoum, Yury Gogotsi. Cation intercalation and high volumetric capacitance of two-dimensional titanium carbide, Science, 2013, 341 (6153), 1502-1505.

[17] Jafar Orangi, Majid Beidaghi. A review of the effects of electrode fabrication and assembly processes on the structure and electrochemical performance of 2D MXenes, Adv. Funct. Mater., 2020, 30 (47), 2005305.

[18] Jizhang Chen, Hao Chen, Minfeng Chen, Weijun Zhou, Qinghua Tian, Ching-Ping Wong. Nacre-inspired surface-engineered MXene/nanocellulose composite film for high-performance supercapacitors and zinc-ion capacitors, Chemical Engineering Journal, 2022, 428, 131380.

[19] Zhonglu Guo, Jian Zhou, Chen Si, Zhimei Sun. Flexible two-dimensional $Ti_{n+1}C_n$ (n = 1, 2 and 3) and their functionalized MXenes predicted by density functional theories, Phys. Chem. Chem. Phys., 2015,17 (23), 15348–15354.

[20] Michael Ghidiu, Maria R. Lukatskaya, Meng-Qiang Zhao, Yury Gogotsi, Michel W. Barsoum. Conductive two-dimensional titanium carbide 'clay' with high volumetric capacitance, Nature, 2014, 516 (7529), 78–81.

[21] Yu Xia, Tyler S. Mathis, Meng-Qiang Zhao, Babak Anasori, Alei Dang, Zehang Zhou, Hyesung Cho, Yury Gogotsi, Shu Yang. Thickness-independent capacitance of vertically aligned liquid-crystalline MXenes, Nature, 2018, 557 (7705), 409–412.

[22] Huan Tang, Wenlong Li, Limei Pan, Kejun Tu, Fei Du, Tai Qiu, Jian Yang, Conor P. Cullen, Niall McEvoy, Chuanfang (John) Zhang. A robust, freestanding MXene-sulfur conductive paper for long-lifetime Li–S batteries. Adv. Funct. Mater., 2019, 29 (30), 1901907.

[23] Y. Yu. Prediction of mobility, enhanced storage capacity, and volume change during sodiation on interlayer-expanded functionalized Ti_3C_2MXene anode materials for sodium-ion batteries, J. Phys. Chem. C., 2016, 120 (10), 5288–5296.

[24] Zheng Ling, Chang E. Ren, Meng-Qiang Zhao, Jian Yang, James M. Giammarco, Jieshan Qiu, Michel W. Barsoum, and Yury Gogotsi. Flexible and conductive MXene films and nanocomposites with high capacitance, PNAS, 2014, 111 (47), 16676-16681.

[25] Yuanming Wang, Xue Wang, Xiaolong Li, Yang Bai, Huanhao Xiao, Yang Liu, Rong Liu, Guohui Yuan. Engineering 3D ion transport channels for flexible MXene films with superior capacitive performance, Adv. Funct. Mater., 2019, 29 (14), 1900326.

[26] Muhammad Boota, Babak Anasori, Cooper Voigt, Meng-Qiang Zhao, Michel W. Barsoum, Yury Gogotsi. Pseudocapacitive electrodes produced by oxidant-free polymerization of pyrrole between the layers of 2D titanium carbide (MXene), Adv. Mater., 2016, 28 (7), 1517-1522.

[27] Armin VahidMohammadi, Jorge Moncada, Hengze Chen, Emre Kayali, Jafar Orangi, Carlos A. Carrero, Majid Beidaghi. Thick and freestanding MXene/PANI pseudocapacitive electrodes with ultrahigh specific capacitance, J. Mater. Chem. A, 2018, 6, 22123-22133.

[28] Chi Chen, Muhammad Boota, Xiuqiang Xie, Mengqiang Zhao, Babak Anasori, Chang E. Ren, Ling Miao, Jianjun Jiang, Yury Gogotsi. Charge-transfer induced polymerization of EDOT confined between 2D titanium carbide layers, J. Mater. Chem. A, 2017, 5 (11), 5260–5265.

[29] Ruizheng Zhao, Zhao Qian, Zhongyuan Liu, Danyang Zhao, Xiaobin Hui, Guanzhong Jiang, Chengxiang Wang, Longwei Yin. Molecular-level heterostructures assembled from layered black phosphorene and Ti_3C_2 MXene as superior anodes for high-performance sodium ion batteries, Nano Energy, 2019, 65, 104037.

[30] Jie Shen, Guozhen Liu, Yufan Ji, Quan Liu, Long Cheng, Kecheng Guan, Mengchen Zhang, Gongping Liu, Jie Xiong, Jian Yang, Wanqin Jin. 2D MXene nanofilms with tunable gas transport channels, Adv. Funct. Mater., 2018, 28 (31), 1801511.

[31] Li Ding, Yanying Wei, Yanjie Wang, Hongbin Chen, Jürgen Caro, Haihui Wang. A two-dimensional lamellar membrane: MXene nanosheet stacks, Angew. Chem. Int. Ed. Engl., 2017, 56 (7), 1825–1829.

[32] Nannan Wu, Qian Hu, Renbo Wei, Xianmin Mai, Nithesh Naik, Duo Pan, Zhanhu Guo, Zhengjun Shi. Review on the electromagnetic interference shielding properties of carbon-based materials and their novel composites: Recent progress, challenges and prospects, Carbon, 2021, 176, 88-105.

[33] Faisal Shahzad, Mohamed Alhabeb, Christine B Hatter, Babak Anasori, Soon Man Hong, Chong Min Koo, Yury Gogotsi. Electromagnetic interference shielding with 2D transition metal carbides (MXenes), Science, 2016, 353 (6304), 1137-1140.

[34] G.K. Kiran, T.V.M. Sreekanth, K. Yoo, J. Kim. Bifunctional electrocatalytic activity of two-dimensional multilayered vanadium carbide (MXene) for ORR and OER, Materials Chemistry and Physics, 2023, 296, 127272.

[35] Yanan Jiang, Tao Sun, Xi Xie, Wei Jiang, Jia Li, Bingbing Tian, Chenliang Su. Oxygen-functionalized ultrathin $Ti_3C_2T_x$MXene for enhanced electrocatalytic hydrogen evolution, Chem. Sus. Chem., 2019, 12 (7), 1368–1373.

[36] Kashif Rasool, Mohamed Helal, Adnan Ali, Chang E. Ren, Yury Gogotsi, Khaled A. Mahmoud. Antibacterial activity of $Ti_3C_2T_x$ MXene, ACS Nano, 2016, 10 (3), 3674–3684.

[37] F. Barja. Bacterial nanocellulose production and biomedical applications, J. Biomed. Res., 2021, 35 (4), 310-317.

[38] Shinichiro Iwamoto, Weihua Kai, Akira Isogai, Tadahisa Iwata. Elastic modulus of single cellulose microfibrils from tunicate measured by atomic force microscopy, Biomacromolecules, 2009, 10 (9), 2571–2576.

[39] Robert J. Moon, Ashlie Martini, John Nairn, John Simonsen, Jeff Youngblood. Cellulose nanomaterials review: structure, properties and nanocomposites, Chemical Society Reviews, 2011, 40 (7), 3941–3994.

[40] A. C. O'Sullivan. Cellulose: the structure slowly unravels, Cellulose, 1997, 4 (3), 173–207.

[41] Djalal Trache, M. Hazwan Hussin, M. K. Mohamad Haafiz, Vijay Kumar Thakur. Recent progress in cellulose nanocrystals: sources and production, Nanoscale, 2017, 9 (5), 1763–1786.

[42] A Pakzad, J Simonsen, RS Yassar. Gradient of nanomechanical properties in the interphase of cellulose nanocrystal composites, Composites Science and Technology, 2012, 72 (2), 314–319.

[43] Denilson da Silva Perez, Suzelei Montanari, Michel R. Vignon. TEMPO-mediated oxidation of cellulose III, Biomacromolecules, 2003, 4 (5), 1417–1425.

[44] Jin Huang, Alain Dufresne, Ning Lin. Introduction to nanocellulose, Nanocellulose: from Fundamentals to Advanced Materials, 2019, 1-20.

[45] Tsuguyuki Saito, Satoshi Kimura, Yoshiharu Nishiyama, Akira Isogai. Cellulose nanofibers prepared by TEMPO-mediated oxidation of native cellulose, Biomacromolecules, 2007, 8 (8), 2485–2491.

[46] Lars Wågberg, Gero Decher, Magnus Norgren, Tom Lindström, Mikael Ankerfors, Karl Axnäs. The build-up of polyelectrolyte multilayers of microfibrillated cellulose and cationic polyelectrolytes, Langmuir, 2008, 24 (3), 784–795.

[47] Wenshuai Chen, Haipeng Yu, Sang-Young Lee, Tong Wei, Jian Lia, Zhuangjun Fan. Nanocellulose: a promising nanomaterial for advanced electrochemical energy storage, Chemical Society Reviews, 2018, 47 (8),2837–2872.

[48] M. Iguchi, S. Yamanaka, A. Budhiono. Bacterial cellulose – a master piece of nature's arts, Journal of Materials Science, 2000, 35 (2), 261–270.

[49] Ichiro Sakurada, Yasuhiko Nukushina, Taisuke Ito. Experimental determination of the elastic modulus of crystalline regions in oriented polymers, J. Polym. Sci., 1962, 57, 651–660.

[50] Lin Gan, Jinglu Liao, Ning Lin, Chenglong Hu, Hualin Wang, Jin Huang. Focus on gradient-wise control of the surface acetylation of cellulose nanocrystals to optimize mechanical reinforcement for hydrophobic polyester-based nanocomposites, ACS Omega, 2017, 2 (8), 4725–4736.

[51] Joshua M. Passantino, Alexander D. Haywood, Joyanta Goswami, Virginia A. Davis. Effects of polymer additives and dispersion state on the mechanical properties of cellulose nanocrystal films, Macromolecular Materials and Engineering, 2017, 302 (4), 1600351.

[52] Qingyuan Niu, Kezheng Gao, Ziqiang Shao. Cellulose nanofiber/single-walled carbon nanotube hybrid non-woven macrofiber mats as novel wearable supercapacitors with excellent stability, tailorability and reliability, Nanoscale, 2014, 6, 4083–4088.

[53] Chuanyin Xiong, Congmin Zheng, Shuangxi Nie, Chengrong Qin, Lei Dai, Yongjian Xu, Yonghao Ni. Fabrication of reduced graphene oxide-cellulose nanofibers-based hybrid film with good hydrophilicity and conductivity as electrodes of supercapacitor, Cellulose, 2021, 28 (6), 3733–3743.

[54] Yu Jin Kang, Sang-Jin Chun, Sung-Suk Lee, Bo-Yeong Kim, Jung Hyeun Kim, Haegeun Chung, Sun-Young Lee, Woong Kim. All-solid-state flexible supercapacitors fabricated with bacterial nanocellulose papers, carbon nanotubes, and triblock-copolymer ion gels, ACS Nano, 2012, 6 (7), 6400–6406.

[55] Keun-Ho Choi, Jong-Tae Yoo, Chang-Kee Lee, Sang-Young Lee. All-inkjet-printed, solid-state flexible supercapacitors on paper, Energy Environ. Sci., 2016, 9, 2812–2821.

[56] Qifeng Zheng, Zhiyong Cai, Zhenqiang Ma, Shaoqin Gong. Cellulose nanofibril/reduced graphene oxide/carbon nanotube hybrid aerogels for highly flexible and all-solid-state supercapacitors, ACS Appl. Mater. Interfaces, 2015, 7 (5), 3263–3271.

[57] Xiao Feng, Xijun Wang, Ming Wang, Shenghui Zhou, Chao Dang, Cunzhi Zhang, Yian Chen, Haisong Qi. Novel PEDOT dispersion by in-situ polymerization based on sulfated nanocellulose, Chemical Engineering Journal, 2021, 418, 129533.

[58] Qingjin Fu, Yanyun Wang, Shuaibo Liang, Qian Liu, Chunli Yao. High-performance flexible freestanding polypyrrole-coated CNF film electrodes for all-solid-state supercapacitors, J. Solid State Electrochem., 2020, 24 (3), 533–544.

[59] Wenzheng Zheng, Ruihua Lv, Bing Na, Hesheng Liu, Tianxiang Jin, Dingzhong Yuan. Nanocellulose-mediated hybrid polyaniline electrodes for high performance flexible supercapacitors, J. Mater. Chem. A, 2017, 5, 12969–12976.

[60] Simon Leijonmarck, Ann Cornell, Göran Lindbergh, Lars Wågberg. Flexible nano-paper-based positive electrodes for Li-ion batteries-Preparation process and properties, Nano Energy, 2013, 2 (5), 794–800.

[61] Yuanyuan Li, Hongli Zhu, Fei Shen, Jiayu Wan, Steven Lacey, Zhiqiang Fang, Hongqi Dai, Liangbing Hu. Nanocellulose as green dispersant for two-dimensional energy materials, Nano Energy, 2015, 13, 346–354.

[62] Jeong-Hoon Kim, Jung-Hwan Kim, Eun-Sun Choi, Hyung Kyun Yu, Jong Hun Kim, Qinglin Wu, Sang-Jin Chun, Sun-Young Lee, Sang-Young Lee. Colloidal silica nanoparticle-assisted structural control of cellulose nanofiber paper separators for lithium-ion batteries, J. Power Sources, 2013, 242, 533–540.